

The Shear Strength of Rock and Rock Joints

N. BARTON*

Rock joints exhibit a wide spectrum of shear strength under the low effective normal stress levels operating in most rock engineering problems. This is due to the strong influence of surface roughness and variable rock strength. Conversely, under the high effective normal stress levels of interest to tectonophysicists the shear strength spectrum of joints and artificial faults is narrow, despite the wide variation in the triaxial compression strength of rocks at fracture. In Part I of this review, empirical non-linear laws of friction and fracture are derived which explain this paradoxical behaviour and which can be used to predict or extrapolate shear strength data over the whole brittle range of behaviour.

Under higher confining pressures the behaviour of rock ceases to be brittle as the brittle-ductile transition is reached. Expressions are derived which quantify this condition and explain the variable transition behaviour of rocks as dissimilar as limestone and shale. At still higher confining pressures the Mohr envelopes describing failure of intact rock eventually reach a point of zero gradient on crossing a certain line, defined here as the critical state line. This critical state is associated with a critical effective confining pressure for each rock. It appears that the dilation normally associated with the shearing of non-planar joints and faults may be completely suppressed if the applied stress reaches the level of the critical effective confining pressure.

The empirical laws of friction and fracture were developed during a review of laboratory-scale testing on rock and rock joints. In Part II of this review these laws are applied to the interpretation of full-scale features. The following topics are investigated; the conjugate shear angle of shear joints and faults, the scale effect on frictional strength, the lack of correlation between stress drops measured in laboratory-scale faulting experiments and those back-calculated from major earthquakes, the strength corrosion caused by moisture, and finally the possible effect of fault dilation and water pressure changes at shallow depth in the crust.

INTRODUCTION

As recently as ten years ago Brace & Byerlee [1] suggested that the coefficient of friction relevant to a particular geologic situation could not be predicted to within better than a factor of two. This pessimistic observation is understandable when one considers the great range of stress to which rock and rock joints are subjected in the various engineering disciplines. In many rock engineering problems, the maximum effective normal stress acting across those joints considered critical for stability will lie in the range 0.1–2.0 MN/m² (1–20 kg/cm²). However, tectonophysicists are generally interested in effective stress levels three orders of magnitude larger than this, for example 100–2000 MN/m² (1–20 kbars).

One of the most surprising conclusions arrived at as a result of high pressure triaxial tests on intact rock is the *apparent* lack of correlation between the fracture strength of the intact rock and the frictional strength of the resulting fault. Byerlee [2] has even gone so far as to suggest that the frictional strength of faults developed through intact rock may be the same for all rocks, independent of lithology.

At first sight there certainly appear to be reasonable grounds for his suggestion. Figure 1 shows that the peak shear strength of artificial faults (and tension fractures) in a variety of rocks falls within a *relatively* narrow zone when the effective normal stress is of the same order or greater than the unconfined compression strength of the rocks concerned. However, rock mechanics experience under low effective normal stress levels indicates that the shear strength of joints can vary within relatively wide limits as indicated in Fig. 2.

*Norwegian Geotechnical Institute, Oslo, Norway.

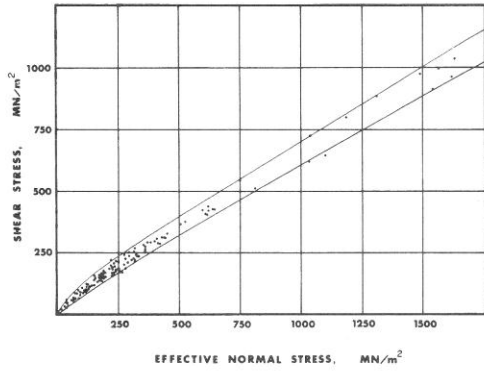


Fig. 1. The shear strength of faults and tension fractures in rock under high effective normal stress. Data from Byerlee [2,5,6] for Westerly granite, Solenhofen limestone, Oak Hall limestone, Nahant gabbro, Spruce Pine dunite, Cabramurra serpentinite, and Weber sandstones—with and without pore pressures.

The obvious question that arises from a study of these two figures is whether the widely different behaviour can actually be governed by the same frictional law, or whether two fundamentally different behaviour patterns are present, one for low stress and the other for high stress. Furthermore, to what extent is frictional strength related to the fracture strength of intact rock?

It will be shown in the following pages that the frictional strength of interlocking rock surfaces (joints, faults, fractures, etc.) is actually governed by the same basic law, possibly for the whole range of brittle behaviour. The frictional strength for effective normal stress levels as low as 0.01 kN/m² (10⁻⁴ kg/cm²) up to more than 1000 MN/m² (10 kbars) can apparently be

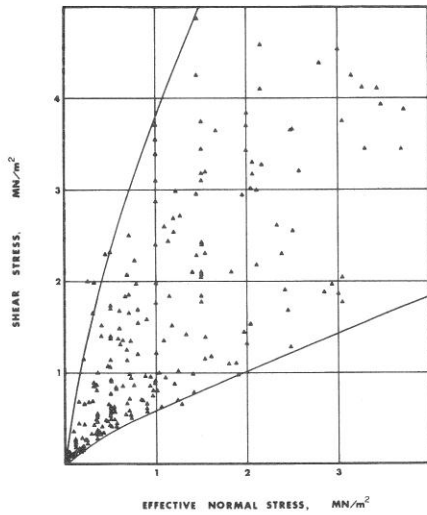


Fig. 2. The peak shear strength of unfilled rock joints from the published results of direct shear tests performed in the laboratory and *in situ* (see [18] for references).

explained according to the results of shear tests performed so far. In physical terms this stress range can be visualized as a depth below surface varying from less than 1 mm up to 40–50 km.

This extreme stress range is bounded at the lower end by *tilting tests*, using laboratory specimens containing a through-going joint and letting the self-weight of the upper half of the jointed specimens provide the shear and normal stress. Sliding occurs when the joint is steeply inclined. The coefficient of friction (μ) may be in excess of 10 under these extremely low stress conditions.

The stress range is bounded at the upper end by the *brittle-ductile transition pressure* [3–6]. Byerlee's results indicate that at room temperature, the transition pressure is that at which the stress required to form a fault surface (*fracture strength*) is equal to the stress required to cause sliding on the fault surface (*frictional strength*). For granite, the coefficient of friction (μ) at the brittle-ductile transition pressure appears to be only about 0.6, even for rough-surfaced faults.

Recent attempts to explain and predict the shear resistance of non-planar rock joints seem to have been based on the observed dilatant behaviour of granular material such as sand. Newland & Allely [7] developed an equation of the following type:

$$\tau = \sigma_n \tan (\Phi_b + i) \quad (1)$$

to denote the maximum shear strength τ of a granular mass when under an effective normal stress σ_n . The angle i was the average angle of deviation of particle displacements from the direction of the applied shear stress, and Φ_b was the angle of frictional sliding resistance between particles. Rowe *et al.* [8] developed the same relationship from energy considerations.

Patton [9,10] and Goldstein *et al.* [11] also used equation (1) to represent the shear strength of irregular rock surfaces and broken rock when tested at low normal stresses. At high normal stresses it was assumed that the Coulomb relationship:

$$\tau = c + \sigma_n \tan \Phi \quad (2)$$

would be valid, since most of the irregularities would be sheared off. The resulting bi-linear envelope has been widely used for interpreting recent test results. The recognition that the shear strength of an irregular rock surface can be zero at zero normal stress represents a very big improvement over the earlier assumption of linear (c, Φ) characteristics.

The existence of curved peak strength envelopes for *intact* rock has been known for many years, as shown by Terzaghi [12]. However, it seems to be only recently that curved envelopes for rock *discontinuities* have been measured and understood. Jaeger [13], Krsmanović & Langof [14], Lane & Heck [15], Patton [9] and Byerlee [5] are among those who first obtained curved relationships between τ and σ_n for a variety of surfaces. It is probable that if more investigators had been interested in low levels of normal stress or alternatively in

very large ranges of normal stress, there would by now be universal acceptance of a fundamentally non-linear shear strength envelope for non-planar rock joints.

The strength components Φ_b and i appearing in equation (1) are usually termed the "basic angle of friction" and the "effective roughness" or " i value" for the case of rock joints. Unfortunately the geometrical component i for a given joint surface is difficult to estimate without performing shear tests. Patton [9] suggested that only the *first-order* irregularities would contribute to the shear strength of joints beneath natural slopes, since slope creep and weathering would probably cause failure of the smaller scale asperities.

However, below the surface-weathered zone all scales of roughness are likely to be important, as emphasised later by Patton & Deere [16].

The development of a satisfactory empirical relationship which can explain *frictional* behaviour both for low and high stress levels forms the subject of the following pages. Its performance in predicting the shear strength of faults developed under high pressure triaxial tests is reviewed in subsequent pages, based on the discovery of a simple relationship between *frictional* strength and *fracture* strength. The shear strength of *intact rock* is investigated in the latter half of Part I, before going on to consider full scale behaviour in the Earth's crust in Part II.

PART I

EMPIRICAL LAW OF FRICTION— LOW STRESS

Figure 3 shows the results of direct shear tests performed on a variety of artificial tension fractures generated through realistic brittle model materials. The left hand diagram (A) shows the total friction angle ($\mu = \arctan \tau/\sigma_n$, where $\tau =$ peak shear strength and $\sigma_n =$ effective normal stress) plotted against the *peak*

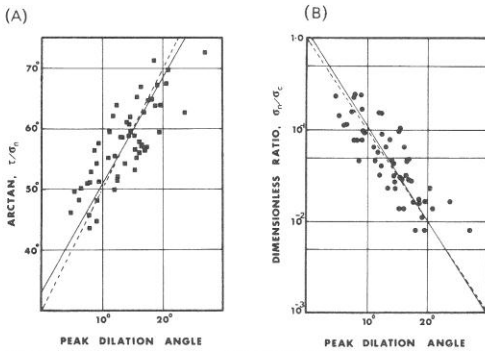


Fig. 3. Peak shear strength results obtained from direct shear tests performed on tension fractures in brittle model materials [17].

*This one-dimensional joint or fault dilation should not be confused with the volumetric dilatancy studied by Brace *et al.* [19] and others.

dilation angle d_n^0 which is defined as the instantaneous inclination of the shearing path at peak strength, relative to the mean plane of the joint or fracture.* Experimental evidence indicates that joints and fractures dilate most strongly when the shear displacement corresponds to the instant of peak shear strength. The peak dilation angle d_n^0 is in fact the maximum dilation angle for a given level of normal stress [18].

The right hand diagram (B) of Fig. 3 also shows the *peak dilation angle* plotted as abscissa. However, the ordinate is the dimensionless ratio σ_n/σ_c relevant to each test, where $\sigma_c =$ the *uniaxial compression strength* of the material. The solid lines extrapolated through the scatter of data are the best-fit lines obtained by the method of least squares. A dotted line is drawn in each diagram, involving a small rotation from the best fit line. The modified lines were drawn so that the following simple relationships could be approximated:

$$\tau/\sigma_n = \tan(2d_n + 30^\circ) \quad (3)$$

$$d_n = 10 \log_{10}(\sigma_c/\sigma_n). \quad (4)$$

The *basic friction angle* ϕ_b for the model materials ranged from 28.5° to 31.5° ($\phi_b =$ residual shear strength of flat non-dilatant rock surfaces, dry or wet). The majority of *unweathered* rock surfaces have values of ϕ_b ranging from 25° to 35° , at least at medium stress levels, for example $\sigma_n = 0.1\text{--}10 \text{ MN/m}^2$ ($1\text{--}100 \text{ kg/m}^2$). Experimental values reported in the literature are summarized in Table 1.

The approximate peak shear strength envelope for the model tension fractures is obtained by eliminating d_n between equations (3) and (4):

$$\tau = \sigma_n \tan\left(20 \log_{10}\left(\frac{\sigma_c}{\sigma_n}\right) + 30^\circ\right). \quad (5)$$

It has been found that for low and medium stress levels this equation gives a close approximation to the *peak shear strength* of interlocking rough-surfaced joints, tension fractures and artificial faults. In fact, if the *unconfined compression strength* (σ_c) of a rock is known, and the interlocking rock surfaces are unweathered (as would be the case for an artificial fault induced in a triaxial test on intact rock), then the peak shear strength envelope can actually be predicted, as shown in Fig. 4. Other examples of strength prediction were given by Barton [18], so will not be reviewed here.

Effect of surface roughness

Equation (5) can be modified to incorporate different degrees of surface roughness. At the smoothest end of the spectrum, the logarithmic function describing the shear strength contribution of asperities must obviously disappear, leaving the linear function:

$$\tau = \sigma_n \tan \phi_b. \quad (6)$$

On the other hand, the roughest end of the spectrum seems to be correctly described by the coefficient (20)

TABLE 1. BASIC FRICTION ANGLE FOR VARIOUS ROCKS, OBTAINED FROM SAND-BLASTED, ROUGH-SAWN AND RESIDUAL SURFACES (1 MN/m² = 10 kg/cm²)

Rock	Moisture	σ_n (MN/m ²)	ϕ_b^0	References ^a
Amphibolite	dry	0.1-4.2	32	a
Basalt	dry	0.1-8.5	35-38	b
	wet	0.1-7.9	31-36	b
Conglomerate	dry	0.3-3.4	35	c
Chalk	wet	0-0.4	30	d
Dolomite	dry	0.1-7.2	31-37	b
Gneiss (schistose)	wet	0.1-7.2	27-35	b
	dry	0.1-8.1	26-29	b
Granite (f.g.)	wet	0.1-7.9	23-26	b
	dry	0.1-7.5	31-35	b
Granite (c.g.)	wet	0.1-7.4	29-31	b
	dry	0.1-7.3	31-35	b
Limestone	wet	0.1-7.5	31-33	b
	dry	0-0.5	33-39	e
Limestone	wet	0-0.5	33-36	e
	dry	0.1-7.1	37-40	b
	wet	0.1-7.1	35-38	b
	dry	0.1-8.3	37-39	b
Porphyry	wet	0.1-8.3	35	b
	dry	0-1.0	31	f
Sandstone	dry	4.1-13.3	31	f
	wet	0-0.5	26-35	e
	wet	0-0.5	25-33	e
	wet	0-0.3	29	g
Shale	dry	0.3-3.0	31-33	c
	dry	0.1-7.0	32-34	b
	wet	0.1-7.3	31-34	b
	wet	0-0.3	27	g
Siltstone	wet	0-0.3	31	g
	dry	0.1-7.5	31-33	b
Slate	wet	0.1-7.2	27-31	b
	dry	0-1.1	25-30	f

^a(a) Wallace *et al.* [20]; (b) Coulson [21]; (c) Krsmanović [22]; (d) Hutchinson [23]; (e) Patton [9]; (f) Barton [24]; (g) Ripley & Lee [25].

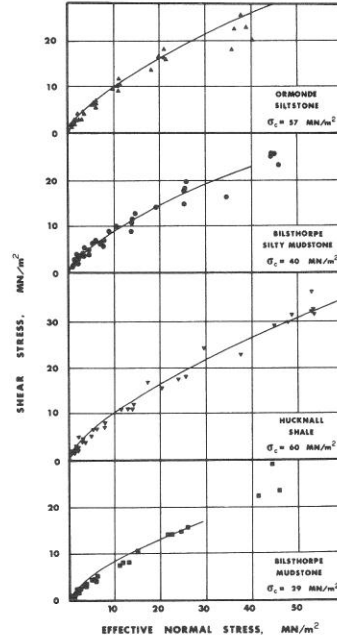


Fig. 4. Plotted points represent the shear strength of artificial faults formed during triaxial tests on 4 coal measure rocks [26]. The unconfined compression strengths (σ_c) measured at zero confining pressure are given in each case. The values were substituted in equation (5) to give the predicted peak shear strength envelopes.

appearing in equation (5). Joints of intermediate roughness are in fact found to have intermediate values of the coefficient. The generalized form of equation (5) is given below,

$$\tau = \sigma_n \tan \left(JRC \log_{10} \left(\frac{JCS}{\sigma_n} \right) + \phi_b \right). \quad (7)$$

The *joint roughness coefficient* (*JRC*) represents a sliding scale of roughness which varies from approx 20 to 0, from the roughest to the smoothest end of the spectrum. The *joint wall compressive strength* (*JCS*) is equal to the unconfined compression strength (σ_c) of the rock if the joint is unweathered, but may reduce to approx (1/4 σ_c) if the joint walls are weathered. Barton and Choubey [27] describe how the (*JCS*) value can be estimated in the field or in the laboratory using a Schmidt hammer.

The physical appearance of equation (7) for different values of the joint roughness coefficient (*JRC*) is seen from Fig. 5. The shear strength envelopes for rough, undulating joints (class A) are steeply inclined at low effective normal stress levels. However, in view of the safety requirements of rock engineering structures, it has been suggested that values of $\arctan \tau/\sigma_n$ larger than 70° and any possible ‘cohesion’ intercept should be discounted, hence the curvi-linear envelopes in the

left hand diagram of Fig. 5. The linear portion is used when $JCS/\sigma_n \geq 100$.

The joint wall compressive strength (*JCS*) is seen from Fig. 5 to be a very important parameter in the shear strength of rough joints when stress levels are low as in most rock engineering problems. The wide spectrum of results predicted for rough-undulating class A joints ($JCR = 20$) is very similar to the scatter found in practice (see Fig. 2). Joints with lower degrees of roughness are progressively less affected by the value of (*JCS*), since asperity failure plays less and less role as the joint roughness coefficient (*JRC*) reduces to zero. Mineralogy (ϕ_b) will increasingly dominate the behaviour at the smooth end of the spectrum.

A very important conclusion can be drawn from Fig. 5. Since the compressive strength of the joint wall is an important component of the shear strength, any process that causes a reduction in this compressive strength should result in reduced shear strength. Increased *weathering*, *moisture content*, *time of failure*, and *scale* cause a marked reduction in the compressive strength of rocks, and hence may also cause a reduction in the peak shear strength of joints. Rough-undulating joints should be most affected and smooth-planar joints least of all. Published results concerning weathered and saturated joints, which were reviewed by Barton [18]

The Shear Strength of Rock and Rock Joints

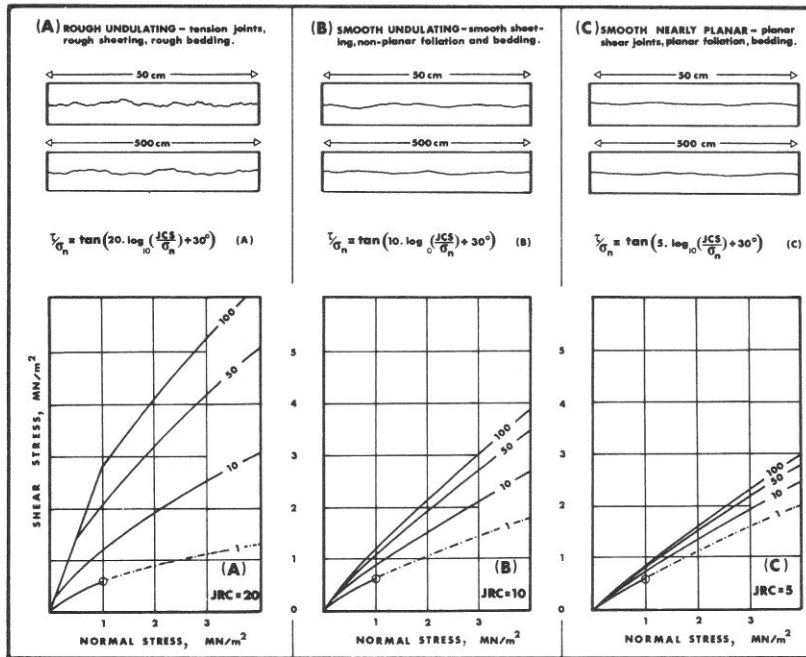


Fig. 5. Classification of roughness and prediction of shear strength for non-planar rock joints. For simplicity ϕ_b is assumed to be 30° throughout. Each curve is numbered with the appropriate value of (JCS), in units of MN/m^2 .

suggest that this hypothesis may be essentially correct. It will be shown later that the scale effect—a very important parameter for *in-situ* prediction—also fits well into the above hypothesis.

Shear strength prediction at low stress

Figure 6 shows the generalized peak shear strength criterion, equation (7), in graphical form as a semi-log plot. The sloping lines which radiate out from the 'origin' ($\phi_b = 30^\circ$ assumed here) represent the peak shear strength for surfaces with roughness coefficients (JRC) equal to 1, 5, 10, 15, 20, and 25. The open circles which mostly cluster between (JRC) values of 18 and 25 are the data points obtained from Fig. 3, and represent the peak shear strength of tension fractures in brittle model materials.

The low stress side of the diagram (JCS/σ_n from 10^2 to 10^6) shows a series of dotted lines, each of them drawn between the results of 2 shear tests performed on the same laboratory joint specimen, which were mostly of $10\text{ cm} \times 10\text{ cm}$ in area. The 10 pairs of data shown here are relevant to 10 specimens containing fairly smooth, planar joints in a granitic intrusive rock, aplite.

Three tilting tests were performed on each of these specimens before shearing under higher stress levels in a shear box. In most of the tilting tests, sliding began when the joints were inclined at between 50° and 70° , as shown by the points at the low stress side of Fig.

6. The effective normal stress is so low when sliding occurs that no damage results. Tilting tests can therefore be repeated over and over again without reducing the strength. The mean (JCS) value for this set of joints was 122.5 MN/m^2 (1225 kg/cm^2), and the effective normal stress when sliding occurred was mostly between 0.08 and 0.2 kN/m^2 ($0.0008\text{--}0.002\text{ kg/cm}^2$).

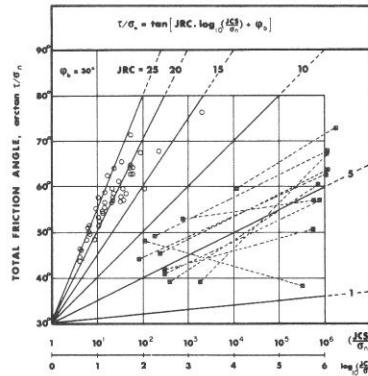


Fig. 6. The empirical law of friction for rock joints in graphical form. Open circles represent the data for model tension fractures obtained from Fig. 3. The dotted lines connect pairs of shear tests performed on the same rock joint, first at very low stress, then at conventional normal stress levels.

The data points plotted at the high stress end of the dotted lines (JCS/σ_n from 10^2 to 10^4) are the results of the shear tests performed in a conventional direct shear box, using the same joints as before. Ignoring the inevitable scatter caused by occasional lack of interlock, it is seen that the results of a shear test under very low stress levels can give quite a fair estimate of the shear strength at stress levels four orders of magnitude greater, if the low stress results are extrapolated using the appropriate (JRC) value.

Naturally, if conventional shear tests have already been performed, it is a simple matter to back-calculate (JRC) from the results using equation (7), provided that (JCS) and ϕ_b can be estimated. In theory, a single back-calculation will produce the correct peak strength envelope for extrapolation purposes. The reliability is obviously improved if more than one test is performed.

Shear strength at extremely low stress

The experimental data shown in Fig. 2 shows several plotted points with values of arctan (τ/σ_n) of about 80° when the effective normal stress is below 0.5MN/m^2 (5 kg/m^2). Some of the other high values reported in the literature are shown in Table 2. The direct shear tests and tilting tests performed on rough interlocking joints by Barton & Choubey [27] have in fact shown values of arctan (τ/σ_n) in excess of 88° when the effective normal stress is lower than about 0.05 kN/m^2 (0.0005 kg/cm^2).

A shear strength envelope for rough joints having a vertical tangent at or close to the shear stress axis instead of a 'cohesion' intercept is inherently satisfying as a limiting condition since, unless asperities are inclined at more than about 60° to the mean plane of the joint ($\phi_b + 60^\circ \geq 90^\circ$), a genuine cohesion intercept as exhibited by intact rock seems unlikely.

The use of a 'cohesion' intercept for rock joints is inherently dangerous, even if the extrapolation is made from the mean effective normal stress level appropriate to the particular engineering problem.

A region of shear strength that does not exist will have been assumed in the design, since in most problems the range of effective normal stress extends to

zero. The Coulomb concept of cohesion (c) and friction (ϕ) is really no more than a simple mathematical convenience since 'cohesion' is not a constant, either for rock or for soils.

Examination of Fig. 6 leads to an intriguing question concerning the peak shear strength of rock surfaces at extremely low stress levels. Is it possible that the *peak shear strength envelopes of all natural mating rock surfaces* display vertical tangency at 'zero' effective normal stress, assuming that the rock surfaces are not optically flat or finely polished? A linear extrapolation of Fig. 6 to even lower stress levels suggests that this might be true, at least when there is measurable non-planarity (i.e. $JRC > 5$). On a microscopic scale even 'smooth' rock surfaces in contact probably resemble interlocking mountainous terrains.

EMPIRICAL LAW OF FRICTION— HIGH STRESS

The empirical law of friction, equation (7), indicates that when joints are unweathered, the *unconfined* compression strength (σ_c) can be substituted for the joint wall compressive strength (JCS). This form of the equation works well at the low stress levels appropriate to most rock engineering problems, provided of course that the joints are unweathered. However, if the effective normal stress is high, or if the unconfined compression strength of the rock is low, the dimensionless ratio (σ_c/σ_n) reduces towards unity, and the resultant shear strength *theoretically* approaches the value given by equation (6), i.e. $\tau = \sigma_n \tan \phi_b$.

Contact area and confining effect

Attempts to fit equation (7) to the results of triaxial shearing tests on artificial faults performed at stress levels of several hundred MN/m^2 , indicate that there is an increasing error between prediction and test results, if the effective normal stress (σ_n) exceeds the rock's *unconfined* compressive strength (σ_c). The measured shear strength is always appreciably *higher* than that predicted.

TABLE 2. MAXIMUM VALUES OF PEAK (τ/σ_n) MEASURED ON JOINTS DURING TESTS AT LOW NORMAL STRESS ($1\text{ MN/m}^2 = 10\text{ kg/cm}^2$)

Description of discontinuity	τ/σ_n (MN/m^2)	arctan (τ/σ_n)	Reference
Limestone: slightly rough bedding surface	0.68/0.16	77°	Goodman [28]
	0.66/0.21	72°	
	1.68/0.60	71°	
Limestone: rough bedding surface	0.68/0.31	66°	Goodman [28]
	2.07/0.68	72°	
Shale: closely jointed seam in limestone	0.06/0.02	71°	Goodman [28]
	0.06/0.02	70°	
Quartzite, gneiss and amphibolite discontinuities beneath natural slopes:	—	80°	Paulding [29]
	—	75°	
Granite: rough, undulating, artificial extension fractures	0.45/0.15	72°	Rengers [30]
	0.92/0.35	69°	

The Shear Strength of Rock and Rock Joints

The reason for the discrepancy is presumably due to the effect of confinement on the compressive strength of rock asperities. At the low stress levels appropriate to most rock engineering problems the contact area between joint walls is extremely small [31]. The strength of the asperities can therefore be considered as the unconfined strength. However, as the level of (σ_n) approaches the value of (σ_c), the area of contact across the joint or fault increases, probably as a result of elastic displacement and possible local failure of any mismatching asperities.

The increasing contact area presumably causes the compressive strength of the asperities themselves to increase due to the more effective confinement. If the (JCS) value appearing in equation (7) develops into the *confined* compression strength of the rock which is equal to the differential stress ($\sigma_1 - \sigma_3$), then equation (7) can apparently be generalized as follows:

$$\tau = \sigma_n \tan \left(JRC \log_{10} \left(\frac{\sigma_1 - \sigma_3}{\sigma_n} \right) + \phi_b \right) \quad (8)$$

where σ_1 is the axial stress at failure, and σ_3 is the effective confining pressure. When $\sigma_3 = 0$, equation (8) has the same form as equation (7). Preliminary, but rather persuasive experimental evidence for the validity of equation (8) will now be given.

Preliminary review of experimental data

Figure 7 shows the results of triaxial compression tests performed on intact cylinders of Weber sandstone by Byerlee [2]. Figure 8 shows the results of the subsequent frictional tests performed on the faults induced

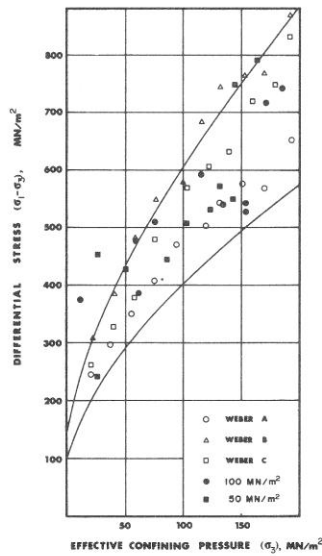


Fig. 7. Differential stress at failure as a function of effective confining pressure for Weber sandstones A, B and C after Byerlee [2]. The solid symbols represent the results of tests with pore pressures. The curved envelopes are explained in the text.

by failure of the intact cylinders. Byerlee calculated the normal and shear stresses for sliding on the fault surfaces from the axial load, confining pressure and fault angle data using the following well known transformations:

$$\tau = \frac{1}{2}(\sigma_1 - \sigma_3) \sin 2\beta \quad (9)$$

$$\sigma_n = \frac{1}{2}(\sigma_1 + \sigma_3) - \frac{1}{2}(\sigma_1 - \sigma_3) \cos 2\beta \quad (10)$$

where β is the angle the fault makes with the major effective principal stress σ_1 . The experimental data shown in Fig. 7 was analysed by measuring the coordinates from Byerlee's original figures. Values of (σ_n) appropriate to the differential stress ($\sigma_1 - \sigma_3$) were estimated using equation (10), with an assumed fault angle (β) of 30° which appears to be a reasonable mean value according to the results of high pressure triaxial tests on rock. Mogi [4, 32] shows values of β that range from about 20° to 35° , while Raleigh & Paterson [33] show values between 25° and 39° , with an average value of 31° . The angle is found to increase with confining stress if the shear strength envelope is curved, as predicted by the Mohr relation:

$$\beta = 45^\circ - \phi/2 \quad (11)$$

where ϕ is the inclination of the Mohr envelope at the point of tangency.

The experimental values of ($\sigma_1 - \sigma_3$) and the values of (σ_n) as estimated above were substituted in equation (8) for each of the test results shown in Fig. 7. An appropriate (JRC) value of 20 and a (ϕ_b) value of 30° were assumed. The predicted peak shear strength of the faults is shown in Fig. 9. The two solid line envelopes drawn in Fig. 9, and the dotted line envelopes drawn through the experimental data in Fig. 8 are identical. Their origin will be explained shortly.

The remarkable agreement between prediction and experiment leaves little doubt that equations (7) and (8) have rather special properties. The predicted data

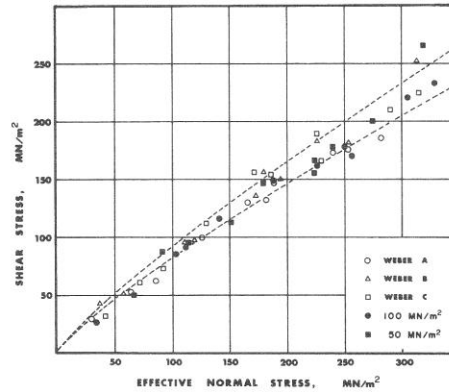


Fig. 8. Shear stress as a function of effective normal stress for sliding on the fault surfaces produced by failure of the Weber sandstones shown in Fig. 7, after Byerlee [2]. The solid symbols represent the results of tests with pore pressures. See text for derivation of the two curves.

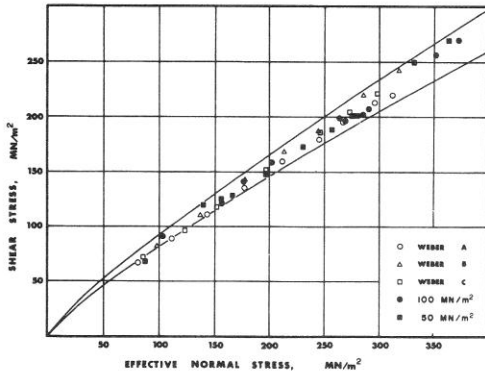


Fig. 9. Predicted peak shear strength of the faults in Weber sandstones according to the proposed frictional law. See text for derivation of the two curves.

actually exhibits less scatter than Byerlee's experimental results and lies completely within the envelope of his data. Yet, it also shows sensitivity to the lower strength of Weber A compared to Weber B (Fig. 7), which results in a slightly lower frictional strength for Weber A than Weber B (Fig. 8).

Byerlee [2] states that "there is no correlation between the fracture strength and the frictional strength of the rock. For instance, Weber B has a consistently higher fracture strength than either Weber A or C, but all three rocks have much the same frictional strength". It will be shown later that the slight error in this assumption may have far reaching consequences on the assumed value of the stress required to reach the brittle-ductile transition pressure within the Earth's crust, considering full scale dimensions.

The above prediction of fault strength depends for its accuracy on correct assumptions regarding the value of (JRC) and (ϕ_b), besides the value of (β) discussed above. Numerous trials have shown that (JRC) = 20 is a very realistic value for rough-surfaced natural joints, and also is relevant to artificial tension fractures in rock (and brittle model material) and to fractures developed under shearing stresses such as in the triaxial apparatus. These fractures are far from smooth before they are sheared beyond peak shear strength. (As residual strength is approached, there is a gradual fall of (JCR), following what may be an initially rapid fall from peak strength).

The assumed value (ϕ_b) of 30° appears from the literature to be very realistic for sandstone. Table 1 shows 6 sets of experimental data for sandstones with the following ranges of ϕ_b : 26°-35°, 25°-33°, 29°, 31°-33°, 32°-34°, 31°-34°. The mean value appears to be approx 31°.

Two-stage prediction of shear strength

The shear strength prediction illustrated in Fig. 9

*Note: the range of σ_c values for Weber sandstones was not given by Byerlee [2], hence the estimates.

was based on experimental results of differential stress ($\sigma_1 - \sigma_3$) at failure as a function of effective confining pressure (σ_3). The fact that this fracture data produced an extremely accurate prediction of frictional strength using equation (8) does nothing more than verify the correctness of the relationship. It would be even more useful if expensive high pressure triaxial testing could be partially replaced by accurate empirical models, both for the fracture strength and the frictional strength. In view of the fact that these small scale triaxial tests can hardly be taken as accurate models of faulting phenomena in the Earth's crust, an empirical model such as equation (8) may be more than justified, particularly since it appears that the scale effect can be taken into consideration, as shown later.

Empirical relationships to describe the compressive strength of intact rock as a function of confining pressure are to be found in great numbers in rock mechanics literature. It is not the intention here to review these, but merely to utilize one of the better ones.

In 1965 Murrell [34] proposed a relation of the following type:

$$\sigma_1 = E\sigma_3^F + \sigma_c \quad (12)$$

where (E) and (F) are constants. Hoek and Bieniawski [35] preferred a dimensionless form, expressing triaxial data in terms of σ_1/σ_c and σ_3/σ_c . Subsequently, Bieniawski [36] expressed equation (12) in dimensionless terms:

$$\frac{\sigma_1}{\sigma_c} = k \left(\frac{\sigma_3}{\sigma_c} \right)^A + 1 \quad (13)$$

where (k) is a constant. This may alternatively be written:

$$\sigma_1 = k\sigma_c \left(\frac{\sigma_3}{\sigma_c} \right)^A + \sigma_c \quad (14)$$

Bieniawski determined the constants (A) and (k) from triaxial tests on more than 400 test specimens consisting of 5 quartzites (91 specimens), 5 sandstones (109 specimens), 1 norite (35 specimens), 4 mudstones (86 specimens), and 4 siltstones (91 specimens). Choosing a constant value for (A) equal to 0.75, he suggested a range of (k) from 3.0 to 5.0 for the above rock types. The highest value (5.0) fits the norite data, while the lowest value (3.0) fits the siltstones and mudstones. It is apparent that if the unconfined compression strength (σ_c) can be estimated, and an appropriate value of (k) chosen, the confined compression strength ($\sigma_1 - \sigma_3$) of many rocks may be estimated reasonably closely.

The two curved envelopes drawn through Byerlee's data [2] for sandstones (see Fig. 7) were obtained from equation (14) using the following assumed values:

- (1) upper envelope (σ_c) = 150 MN/m² (1.5 kbar), (k) = 5.0
- (2) lower envelope (σ_c) = 100 MN/m² (1.0 kbar), (k) = 4.0*

One further assumption is required before equation (14) can be evaluated. We need a simple relation between σ_3 and σ_n . For medium stress levels it is realis-

The Shear Strength of Rock and Rock Joints

tic to assume that $\sigma_3 = \frac{1}{2}\sigma_n$ (approx) as seen from a simple Mohr construction. If the resulting values of $(\sigma_1 - \sigma_3)$ and (σ_n) are substituted in equation (8), with the same values of (JRC) and (ϕ_b) as before, then the 2-curved envelopes shown in Fig. 9 are obtained. The same envelopes are drawn as dotted lines in Fig. 8, which showed Byerlee's experimental data.

Detailed review of experimental data

Further evidence for the validity of equation (8) is required from lithologically dissimilar rocks, since the results obtained from the 3 Weber sandstones A, B and C (dark red, light pink, and grey respectively) may have been fortuitous due to the lithological similarity of the three types.

An ideal set of experimental data is provided by Raleigh & Paterson ([33], Table 1), Mogi ([32], Fig. 10a), Byerlee ([5], Fig. 7) and Byerlee ([6], Figs. 5 and 6). The variation of differential stress $(\sigma_1 - \sigma_3)$ with effective confining pressure (σ_3) for the 6 different rocks is shown in Fig. 10. Wide variations in behaviour are evident.

Figure 11 shows the results of the subsequent frictional tests performed on the faults induced by failure of the intact cylinders. As before, the stresses acting on the fault planes were calculated using the transformation equations (9) and (10).

For the purposes of strength prediction, the experimental data shown in Fig. 10 was analysed as in the case of the Weber sandstones. Values of (σ_n) appropriate to the differential stress $(\sigma_1 - \sigma_3)$ were estimated using equation (10), with an assumed fault angle (β) of 30° as previously discussed. These results were substituted in equation (8) for each of the test results shown in Fig. 10. (JRC) values of 20 and (ϕ_b) values

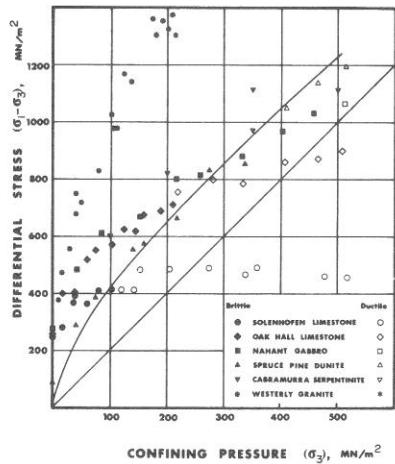


Fig. 10. Differential stress vs confining pressure at fracture, or at 5% strain if specimen was ductile. Closed symbols indicate brittle behaviour, open symbols, ductile (see text for references). The curved envelope is Byerlee's [6] estimate of the brittle-ductile transition. The straight line is explained in the text (see section on critical state).

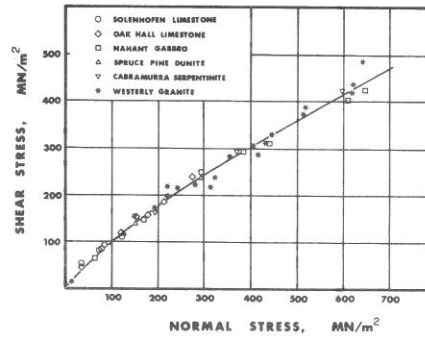


Fig. 11. Shear stress vs normal stress for frictional sliding on the faults developed in the triaxial tests shown in Fig. 10 (after Byerlee [6], Fig. 6).

of 30° were assumed throughout. The predicted peak shear strength of the faults is shown in Fig. 12.

The predicted data are scattered more widely than the experimental data shown in Fig. 11 and also lie a little low. The reasons for this will be analysed in some detail as they are quite instructive.

Firstly, concerning the limestone—the assumption of (β) equal to 30° appears very reasonable. Byerlee [6] observed that “near the pressure of the brittle-ductile transition, the angle that the fault surfaces made with the axis of the specimens was close to 30° for all the rocks”. The limestone specimens, especially the Solenhofen variety, passed through the transition at medium confining pressures, so the assumed 30° cannot be the cause of any major discrepancy.

The most obvious reason for the low predicted shear strength for the faults in the Solenhofen and Oak Hall limestones (Fig. 12) is the ductility. For example, Byerlee's experimental data (Fig. 11) includes no data points for Solenhofen limestone above an effective normal stress of about 120 MN/m^2 (1.2 kbar). Presumably, this is due to the difficulty of defining a fault angle when

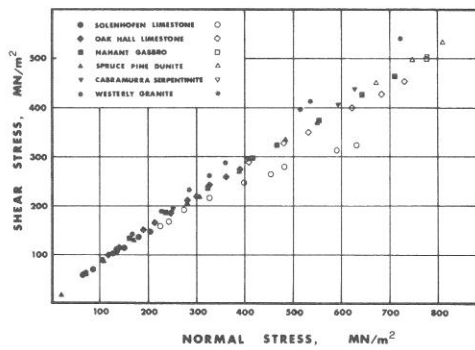


Fig. 12. Predicted peak shear strength of the faults developed in the triaxial tests shown in Fig. 10, according to the proposed frictional law, equation (8). For simplicity ϕ_b was assumed to be 30° in each case. Open symbols were derived from the ductile failure data shown in Fig. 10.

failure is actually ductile. The corresponding predicted points (open symbols in Fig. 12) should therefore be excluded from consideration.

It may be noted from Fig. 11 that at low stress levels—before the onset of ductility—both limestones display higher frictional strength than any of the other rocks, and considerably higher shear strength than that predicted in Fig. 12. The reason for this is the high value of ϕ_b apparently associated with limestones. In Table 1, 6 sets of experimental data for limestones are tabulated, which show the following ranges of ϕ_b : 33°–39°, 33°–36°, 37°–40°, 35°–38°, 37°–39°, 35°. The mean value appears to be approx 37°. If this value had been used in equation (8) for predicting the shear strength of the faults in both limestones in place of 30°, the predicted data would lie exactly 7° higher, as measured from the origin ($\arctan \tau/\sigma_n$ increases 7°). This would bring the limestone predictions very close to the experimental values.

The two-stage method of shear strength prediction employing both equations (8) and (14) can also be used to approximate the experimental results presented in Figs. 10 and 11. Values of (k) ranging from 2.0 (limestone) to 6.0 (granite) together with appropriate assumptions for ϕ_b as outlined above, provide shear strength predictions very close to those actually measured.

THE BRITTLE-DUCTILE TRANSITION

Mogi [4] observed that the fracture behaviour of rocks changes from brittle to ductile with increasing confining pressure, the transition pressure being higher for stronger rocks. For silicate rocks Mogi suggested a linear boundary between brittle and ductile behaviour as below:

$$\sigma_1 - \sigma_3 = 3.4 \sigma_3. \quad (15)$$

In other words, if the confined compression strength is greater than $3.4 \sigma_3$, the behaviour will be brittle, and vice versa. At the same time, Mogi observed that the transition pressure of weaker marbles and limestones was appreciably lower, the transition boundary being curved (concave downward).

Various kinds of silicate rocks apparently have an almost identical coefficient of friction $\mu = 0.65$ ($\arctan \tau/\sigma_n = 33^\circ$) at the transition, while for carbonate rocks the value is frequently over 1.0 ($\arctan \tau/\sigma_n = 45^\circ$) according to Mogi [4]. Shales, which are known to have a higher transition pressure than other silicate rocks, were not included in Mogi's data.

A physical explanation for the phenomenon of the brittle-ductile transition was given by Orowan [3]. He suggested that at a sufficiently high confining pressure, the shear strength of a fault would eventually be as high as the shear stress required to develop the fault through the intact rock. If this was the case, there would be no stress drop when the fault formed. This hypothesis seems to be consistent with the changing

shape of stress-strain curves as the transition to ductile (stable) behaviour is approached.

Byerlee [6] used a simple technique for investigating the brittle-ductile transition. He drew a single curved envelope through collected frictional data for sliding tests on faults (see Fig. 11) and transformed this curved τ, σ_n envelope into σ_1 and σ_3 coordinates using equations (9) and (10). He assumed a fault angle (β) = 30° for the 6 rock types investigated, thereby simplifying the transformation as follows:

$$\sigma_1 - \sigma_3 = 2.31\tau. \quad (16)$$

$$\sigma_3 = \sigma_n - 0.58\tau. \quad (17)$$

The resulting non-linear relationship between the differential stress and the confining pressure is drawn in Fig. 10.

Byerlee reasoned as follows: if Orowan's [3] friction hypothesis for the brittle-ductile transition in rocks was valid, the rock should be brittle if at any confining pressure the differential stress that a rock could support at failure fell above Byerlee's curve (Fig. 10). The rock should be ductile if the differential stress fell below the curve.

The distribution of open and closed symbols shown in Fig. 10 which indicate ductile and brittle failure respectively, proved that the frictional hypothesis was essentially correct.

Variable transition pressures due to ϕ_b values

Significantly, Byerlee [6] did note 'slight departures' from his transition curve, which were accounted for by the "small dependence of friction on rock type". He noted for example, that the transition pressure was slightly lower for the Oak Hall limestone. Byerlee also noted that the transition pressure for shale was very much higher than his curve, "because the frictional shear stress required to cause sliding on surfaces of shale at any given normal stress is very much lower than it is for other rocks". All these interesting observations point to *variable frictional strength* as the chief cause for *variable transition pressure*. A single curve for all rocks is then inadmissible as a general transition boundary between brittle and ductile behaviour.

It thus appears that the potential range of ϕ_b associated with different types of rock may be an important cause of the variable transition pressures observed. As will be shown below, this variable ϕ_b has a marked effect on the theoretical peak shear strength of joints and faults. If, as seems likely, ϕ_b values affect the friction strength of pre-existing faults more than the fracture strength of the intact rock, then low values of ϕ_b will tend to 'delay' the transition, and high values will 'accelerate' it. The pressure at which the transition occurs will also be affected by the confined strength of the rock. The transition pressure should in fact depend on both the value of ϕ_b , and the value of $(\sigma_1 - \sigma_3)$ appropriate to the confining pressure σ_3 .

When ϕ_b has a value different from 30°, all the envelopes drawn in Fig. 6 will be moved up or down the

The Shear Strength of Rock and Rock Joints

ordinate. The focal point of all the envelopes is in fact the value of ϕ_b . The 32 sets of experimental data for ϕ_b given in Table 1 show a common range of 25–35° as mentioned earlier. However, extreme values of 23° (schistose gneiss) and 40° (limestone) are found. Thus, a wide range of shear strength is theoretically possible, even for the same value (JRC) and $(\sigma_1 - \sigma_3)/\sigma_n$.

It is perhaps worth summarizing the experimental details for measuring ϕ_b (Barton, [24]). It is the value of $\arctan(\tau/\sigma_n)$ obtained from *residual* shear tests on flat unweathered rock surfaces which are normally prepared by sawing, but which can conveniently be sand-blasted between tests.

It appears that the value of (ϕ_b) of rock is most closely simulated by these artificial surfaces when shear force displacement characteristics show no appreciable peak, nor fall to residual. (This is analogous to behaviour at the transition.) In addition, the surfaces should not be so smooth that stick-slip oscillations occur, nor so smooth that the frictional resistance rises due to roughening of the smooth surfaces with increased displacement. In other words, the granular texture of the rock should be exposed, but not to the extent that macroscopic interlocking and dilation occur. Sand-blasting of flat sawn surfaces appears to satisfy all these requirements. The surfaces may be dry or wet according to the desired application of the results, i.e. whether the joints are dry or saturated *in situ*. The effect of water on these unpolished, flat surfaces is, however, not so great as one might expect. The results given in Table 1 indicate extreme ranges for saturated samples of 23° (schistose gneiss) to 38° (limestone), and for dry samples: 25° (slate) to 40° (limestone).

Value of $\arctan(\tau/\sigma_n)$ at the transition

If the experimental data presented in Fig. 11 is analysed, it is found that the *lowest values* of $\arctan(\tau/\sigma_n)$ for each of the rock types range from about 33° to 42°, as tabulated below. The lowest values for each rock correspond to those tests performed close to the brittle-ductile transition. In fact, if the data is scrutinized closely, it will be seen that some of the 'brittle' failures plotted in Fig. 10 have not been included by Byerlee in Fig. 11, so some of the values of $\arctan(\tau/\sigma_n)$ at the transition are probably 2° or 3° lower than the values given below:

	τ/σ_n	$\arctan(\tau/\sigma_n)$
Solenhofen limestone	0.90	42°
Oak Hall limestone	0.90	42°
Nahant gabbro	0.66	33°
Spruce Pine dunite	0.81	39°
Cabramurra serpentinite	0.71	35°
Westerly granite	0.65	33°

It may be observed that the above values are strikingly sensitive to the different ϕ_b values to be expected of the given rock types, though perhaps 4° or 5° too high.

Careful analysis of the $(\sigma_1 - \sigma_3)$ vs (σ_3) values for the 'last' brittle failure and the 'first' ductile failure (closed

and open symbols in Fig. 10), indicate that the ratio of $(\sigma_1 - \sigma_3)/\sigma_n$ for an assumed fault angle of 30° averages 1.68 and 1.58 respectively for the 6 rock types. The empirical law of friction, equation (8), would therefore predict values of $\arctan(\tau/\sigma_n)$ that are 4.5° and 4.0° in excess of ϕ_b . Since the 'last' brittle failure and the 'first' ductile failure presumably lie on either side of the brittle-ductile transition, it seems very reasonable to conclude that the shear strength at the transition is governed by following relationship:

$$\theta_t = \phi_b + 2d_n \quad (18)$$

This is of the same form as equation (3). By implication, at high stress levels ($\sigma_n > \sigma_c$), equation (4) can be modified to the following form:

$$d_n = 10 \log_{10} \left(\frac{\sigma_1 - \sigma_3}{\sigma_n} \right) \quad (19)$$

If the above hypothesis is correct, it implies that the peak dilation angle (d_n) for faults sheared at the *brittle-ductile transition* pressure average about 2° for these 6 rock types, with a range of about 1–3°.

THE CRITICAL STATE FOR ROCK

It seems inherently reasonable that when the effective normal stress mobilized on a potential failure plane finally reaches the level of the confined compression strength ($\sigma_n = \sigma_1 - \sigma_3$), the *one-dimensional dilation* normally associated with shearing will be suppressed. If it could be shown that at this same state of stress the *volumetric dilation* was also suppressed, then a significant 'critical state' for rock could be defined. For example, at pressures lower than a certain effective confining pressure volumetric dilation of the type observed by Brace *et al.* [19] would occur, together with the one-dimensional dilation across the mobilized failure surfaces. At higher pressures the signs of both types of dilation would become negative.

So far as the author is aware, there is no experimental data available specifically relating the 2 forms of dilation discussed above. However, a change in sign of the volumetric dilation under high effective confining pressures has been noted, for example by Cornet & Fairhurst [37]. In view of the experimental difficulties a simpler definition of the critical state is required.

The *critical state for initially intact rock* will be defined as the stress condition under which the Mohr envelope of peak shear strength reaches a point of zero gradient. This represents the maximum possible shear strength of the rock. For each rock there will be a *critical effective confining pressure* above which shear strength cannot be made to increase. This pressure is represented by σ_3 in Fig. 13, and the critical point of the envelope is point C.

It is of paramount interest to see how the above definition of the critical state for initially intact rock corresponds with the condition $\sigma_n = \sigma_1 - \sigma_3$ for the mobilized failure surfaces or faults produced in a conventional 'triaxial' apparatus ($\sigma_2 = \sigma_3$). It will be

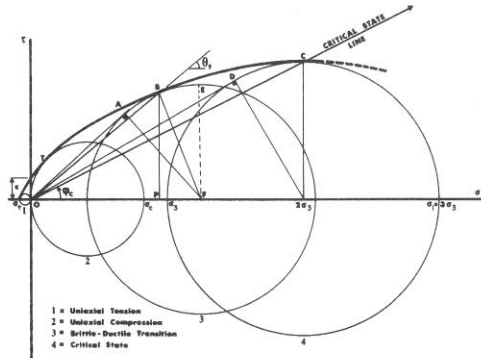


Fig. 13. The proposed critical state is represented by point C. It lies on the critical state line which has a gradient $\tan \phi_c = \frac{1}{2}$. The critical effective confining pressure is equal to σ_3 in this figure.

remembered from equation (19) that $\sigma_n = \sigma_1 - \sigma_3$ theoretically represents the stress condition under which the one-dimensional dilation occurring at peak strength is finally suppressed ($d_n = 0^\circ$).

The normal stress mobilized on the conjugate 45° failure planes $2\beta = 90^\circ$, equation (11), at the critical point C is equal to $\frac{1}{2}(\sigma_1 + \sigma_3)$, where σ_1 and σ_3 represent the effective principal stresses defining the critical state. It follows that if $\sigma_n = \sigma_1 - \sigma_3$ represents the 'critical state' for the mobilized failure surfaces, then:

$$\frac{1}{2}(\sigma_1 + \sigma_3) = \sigma_1 - \sigma_3 \quad (20)$$

or

$$\sigma_1 = 3\sigma_3. \quad (21)$$

Circle No. 4 in Fig. 13 has been drawn with these values. It will be seen that the ultimate shear strength represented by point C is equal to the critical effective confining pressure (σ_3) required to reach the critical state. The normal stress is equal to $2\sigma_3$. The critical state line (OC) will subtend an angle (ϕ_c) given by the following relationship:

$$\tan \phi_c = \frac{\sigma_1 - \sigma_3}{\sigma_1 + \sigma_3} \quad (22)$$

Thus, with $\sigma_1 = 3\sigma_3$, $\tan \phi_c = \frac{1}{2}$ and $\phi_c = 26.6^\circ$.

The tangent point D to the same critical stress circle subtends an angle θ_c , where:

$$\sin \theta_c = \frac{\sigma_1 - \sigma_3}{\sigma_1 + \sigma_3}. \quad (23)$$

From equation (21) it will be seen that $\theta_c = 30^\circ$ ($\sin \theta_c = \frac{1}{2}$). This can be likened to the hypothetical 'internal friction angle' ϕ .

If it can be demonstrated that the stress condition $\sigma_1 = 3\sigma_3$ at peak shear strength does indeed represent the stress condition required to reach the point of maximum shear strength (the top of the Mohr envelope) for rocks, then an important relationship between the behaviour of intact rock and faulted rock will have

been established. It would also help to explain the extremely close fit between experimental data and the empirical law of friction, equation (8), which incorporates the relation $(\sigma_1 - \sigma_3)/\sigma_n = 1$ as one of its limiting conditions.

Review of experimental data

The triaxial test results plotted in Fig. 10 provide an immediate source of data for testing the proposed critical state theory. The straight line drawn in Fig. 10 has the same gradient as represented in equation (21), i.e. $\sigma_1 - \sigma_3 = 2\sigma_3$. It is apparent that the Solenhofen limestone reduces in strength on crossing the critical state line.

Figure 14 shows a dimensionless plot of the same triaxial data together with additional high stress data for Westerly granite obtained from Byerlee ([5], Fig. 8), and Mogi ([32], Table 2). The dimensionless term was obtained by normalizing the differential stress with the unconfined compression strength σ_c . It is apparent from the figure that $\sigma_1 = 3\sigma_3$ is a special condition for the 6 rock types represented. The granite in particular seems to be particularly 'reluctant' to cross the proposed critical state. In passing, it should be noted that the straight lines:

$$\frac{\sigma_1 - \sigma_3}{\sigma_c} = M \sigma_3 / \sigma_1 + 1.0 \quad (24)$$

represent quite good approximations to the shear strength of intact rock up to the critical state condition. The gradients (M) for Solenhofen limestone, Oak Hall limestone, Nahant gabbro and Westerly granite are equal to approx. 3, 7, 9 and 30, respectively. These linear relationships are made use of later.

A large body of experimental triaxial data for rocks was assembled by Mogi [4] from a variety of sources.

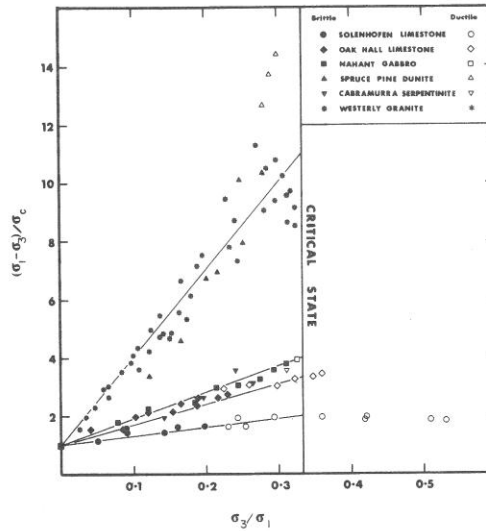


Fig. 14. Dimensionless plot of triaxial data obtained from Fig. 10. The proposed critical state is represented by $\sigma_3/\sigma_1 = 0.333$ at failure.

The Shear Strength of Rock and Rock Joints

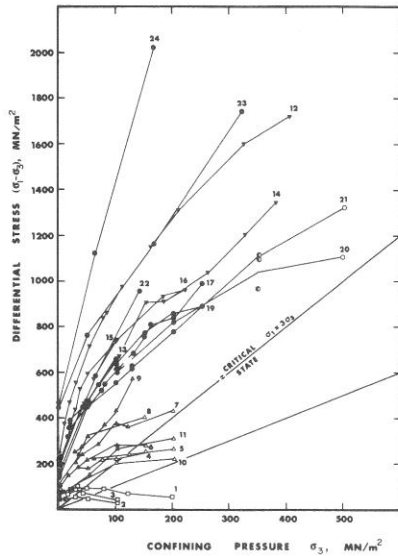


Fig. 15. Triaxial data for dry silicate rocks compiled by Mogi [4], (Fig. 2). All tests were performed at room temperature. Brittle, transitional and ductile behaviours are indicated by closed symbols, half-open symbols and open symbols respectively.

This data is reproduced in Figs. 15 and 16, together with the proposed critical state line. It should be noted that an envelope that reaches zero gradient when plotted in terms of the effective principal stresses σ_1 and σ_3 will have a corresponding point of zero gradient when plotted as a Mohr envelope in terms of the mobilized stresses τ and σ_n .

In general, it appears that $\sigma_1 = 3\sigma_3$ can be taken as a satisfactory approximation to the critical state of these rocks, though small variations should be anticipated. It is of interest to investigate which rocks do not appear to conform based on the evidence of Figs. 10, 15 and 16.

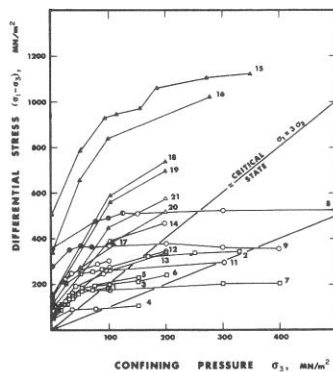


Fig. 16. Triaxial data for dry carbonate rocks compiled by Mogi [4] (Fig. 3). All tests were performed at room temperature. Brittle, transitional and ductile behaviours are indicated by closed symbols, half-open symbols and open symbols respectively.

Firstly, from Fig. 10 it appears that the stronger of the 2 limestones has not reached its critical state at $\sigma_1 = 3\sigma_3$. In Fig. 15 the curves numbered 5, 10 and 11 (and possibly 7), show a continued rise in strength beyond the proposed critical state. These rocks are respectively; Mizuho trachyte, Bartlesville sandstone, Barns sandstone and Tatsuyama tuff. Mogi [4] describes all 4 as porous, with a porosity in the range of 1-10%. In contrast the curves numbered 1, 2 and 3 representing highly porous (> 10%) weak tuffs and andesite do seem to obey the critical state law. The possible reason for this discrepancy is of great interest.

It will be noted from Fig. 15 that the 4 rocks mentioned above, which do not at first sight appear to have reached the critical state (7, 11, 5, 10) are in a ductile state at the highest pressure. If the pore air was unable to drain under high confining pressures due to inefficient pore connection, it would be subjected to a pressure equal to the confining pressure. In fact, the critical state line for undrained tests is represented by $\sigma_1 = 2\sigma_3$. This line is drawn in Fig. 15, and it appears that curves 7, 11, 5, and 10 will satisfy this condition very well. The fact that curves 1, 2 and 3 do satisfy the drained critical state condition is perhaps due to the much greater porosity and greater possibility of internal pore drainage during collapse of these weak porous rocks.

In Fig. 16 there are at least 7 rocks which do not appear to obey the proposed critical state. Curves 2, 3, 5 and 6 represent marbles, and curves 11, 12 and 13 limestones. It would appear that they might well obey the 'undrained' critical state line ($\sigma_1 = 2\sigma_3$), but whether the previous argument concerning pore air can be invoked here, is a matter for conjecture.

The strongest rock represented in Fig. 15 (curve 24, quartzite), is of such high strength that it seems unlikely that its critical state will be reached until extremely high confining pressures, which will probably be in excess of existing experimental capacity. However, some of the medium to high strength rocks such as curve 20 (serpentine) in Fig. 15, and curves 15 and 16 (dolomites) in Fig. 16, do appear to conform.

Prediction of critical effective confining pressure

If the linear relationship represented by equation (24) can be used to extrapolate low pressure triaxial data, then the critical state of these extremely strong rocks can perhaps be estimated, thereby avoiding expensive high pressure tests. It has been shown that the critical state is represented by the following identities: $(\sigma_1 - \sigma_3) = \sigma_n$, $\sigma_1 = 3\sigma_3$. Thus equation (24) can be simplified to give the following relationship:

$$\sigma_3(\text{critical}) = \frac{1}{2} \sigma_c (M/3 + 1.0). \quad (25)$$

It follows that the value of σ_n acting on the mobilized failure planes at the critical state is equal to $2\sigma_3$ (critical).

The extreme gradients (M) of 3 and 30 obtained for Solenhofen limestone and Westerly granite from Fig. 14, suggest values of $\sigma_3(\text{critical})$ of 250 MN/m² (2.5

kbar) and 1320 MN/m² (13.2 kbar) respectively. As will be seen from Figs. 10 and 17, the first value is exactly as found. However, experimental data is not available to test the predicted critical state for the granite. The extremely strong quartzite (Fig. 15, curve 24) has, according to the mean gradient of the 3 available experimental points, a value of σ_3 (critical) of about 3000 MN/m² (30 kbar). Diabase (Fig. 15, curve 23) should have σ_3 (critical) very similar to the Westerly granite represented by curve 12. The dissimilar gradients ($M = 15$ and 30 , respectively) compensate for the higher uniaxial strength of the diabase.

Corresponding behaviour of sands

Before leaving this review of experimental data, it is of great interest to see the way sand behaves under high confining pressures. Vesic & Barksdale [38] conducted triaxial tests on a river sand up to confining pressures of 63 MN/m² (630 kg/cm²). The strength envelope for conventional low pressure tests (below 70 kN/m², 0.7 kg/cm²) was inclined at about 44°, decreasing to about 39° at pressures of about 500 kN/m² (5 kg/cm²). Vesic and Barksdale found that under high confining pressures the envelope is virtually linear, i.e. from about 3 MN/m² (30 kg/cm²) up to the maximum pressure of 63 MN/m² (630 kg/cm²). The overall inclination is almost exactly 30°. Of all the high pressure test results, only two show stresses at failure of $\sigma_1 < 3.0 \sigma_3$. These two exceptions are in the range $3.0 \sigma_3 > \sigma_1 > 2.9 \sigma_3$. Vesic & Clough [39] show similar results, with only one value ($\sigma_1 = 2.97 \sigma_3$) less than the proposed critical state for rock.

In view of the crushing of sand grains and reduction in pore volume that occurs, it seems very reasonable to compare behaviour of sands at very high confining pressures with that of weakly cemented porous rocks. High pressure penetrometer tests in sand can apparently result in 'petrification', the instrument head being

coated with a material resembling a weak rock after extraction from the sand (Holden, 1975, personal communication).

EMPIRICAL LAW OF SHEAR STRENGTH FOR INTACT ROCK

The triaxial strength data for the 6 rock types shown in Fig. 10 show wide variation of behaviour, from the ductile Solenhofen limestone through to the very strong Westerly granite. Mohr envelopes were constructed for both these rocks, and also for the intermediate strength dunite. An example is shown in Fig. 17. Each point of tangency (Nos. 1, 3, 6, 10, 12 and 15) represents the stresses at failure. These values of τ/σ_n were analysed for the three rocks, in an attempt to derive a shear strength law for intact rock incorporating the critical state expression $(\sigma_1 - \sigma_3)/\sigma_n$ which was found to be so relevant for rock joints and faults. An expression of the following type was tested:

$$\tau/\sigma_n = \tan \left(m \log_{10} \left(\frac{\sigma_1 - \sigma_3}{\sigma_n} \right) + \phi_c \right) \quad (26)$$

The angle ϕ_c , defined the slope of the critical state line, and was equal to 26.6° (arctan $\frac{1}{2}$).

It was found that (m) was close to 50 for all 3 rocks over the whole range of stresses from the uniaxial compression stress circle (No. 1 in Fig. 17; No. 2 in Fig. 13), right up to the critical circle, or up to the maximum stress tested in the case of the granite and dunite.

Reversing the procedure and assuming a constant value (m) = 50, the following mean angles were obtained: Westerly granite 25.8°, Spruce Pine dunite 25.4°, Solenhofen limestone 26.7°. For all practical purposes it appears reasonable to assume that the following expression describes the shear strength of intact rock:

$$\tau/\sigma_n = \tan \left(50 \log_{10} \left(\frac{\sigma_1 - \sigma_3}{\sigma_n} \right) + \phi_c \right) \quad (27)$$

where ϕ_c is equal to 26.6°.

The fact that equation (27) fits *correctly inclined curved envelopes to all the stress circles* from uniaxial compression up to, in the case of Solenhofen limestone, the critical stress circle is remarkable, especially when the widely different gradients of granite and limestone are considered (equation (24), Fig. 14). It suggests that the rock 'knows' that it is governed by a critical state where the shear strength will reach a maximum value equal to the critical effective confining pressure—even though this value varies widely between rocks as different as limestone and granite.

Equation (27) is valid down to a stress level equivalent to point T in Fig. 13. It will probably also be valid for negative values of σ_3 , provided that σ_n remains on the positive side of the axis. The low and negative stress portion of the strength envelope between the uniaxial tension and compression circles determines the cohesion intercept (c). From the geometrical relations of Mohr theory it can be shown that the theoretical cohe-

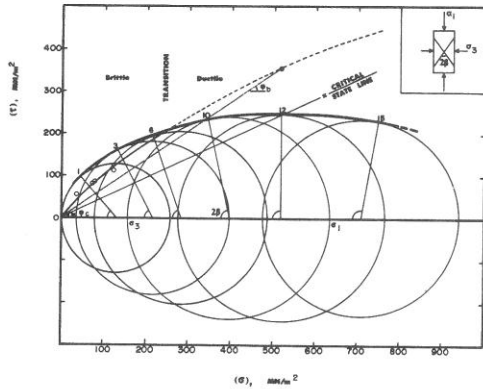


Fig. 17. Mohr envelope for Solenhofen limestone based on data from Fig. 10. The four open circles are the measured shear strength data for faults in the brittle range of behaviour, as plotted by Byerlee [6] (see Fig. 11).

sion intercept obtained by assuming a *linear envelope* in this region is:

$$c = \frac{1}{2} (\sigma_c \times \sigma_t)^{\frac{1}{2}} \quad (28)$$

Isotropic rock properties are assumed. Most rocks have σ_c/σ_t in the range 5–20. If for convenience values of 9 and 16 are assumed, then values of (c) equal to $1/6 \sigma_c$ and $1/8 \sigma_c$ are obtained. These values are clearly conservative estimates, when the curvature of the real envelopes are considered.

The gradient of the theoretical linear envelope between the uniaxial tension and compression circles is given by the following relationship:

$$\sigma_c/\sigma_t = \tan^2 (45^\circ + \phi/2) \quad (29)$$

where ϕ is the theoretical angle of friction in this stress region.

PREDICTION OF TRANSITION BEHAVIOUR

In the light of our knowledge of the peak shear strength of faults through rock up to the transition pressure:

$$\tau/\sigma_n = \tan \left(20 \log_{10} \left(\frac{\sigma_1 - \sigma_3}{\sigma_n} \right) + \phi_b \right), \quad (30)$$

it is now possible to obtain an expression for the apparent stress drop resulting from fracture below the transition pressure. The limiting case occurs at the transition pressure itself. At this point the friction and fracture curves intersect, and the shear stress required to cause fracture of the intact rock is the same as that required to cause sliding on the resulting fault. Thus:

$$\log_{10} \left(\frac{\sigma_1 - \sigma_3}{\sigma_n} \right) = \left(\frac{\phi_b - \phi_c}{30} \right). \quad (31)$$

By implication the peak dilation angle occurring across a fault at the brittle–ductile transition is as follows:

$$d_n = 1/3(\phi_b - \phi_c). \quad (32)$$

This is a very significant expression because it suggests that rocks such as shales with $\phi_b < \phi_c$ will not be dilating at the transition. This may well mean that shales—which are sometimes excluded from the results of high pressure triaxial data because of their unusual behaviour—have reached their critical state before (or simultaneously with) the brittle–ductile transition. Shear tests performed on shale by Maurer [40] suggest values of ϕ_b as low as 22° ($\mu = 0.4$).

If a realistic range of ϕ_b values of 30° – 36° is assumed for the 6 rock types represented in Fig. 10, then equation (31) suggests that at the transition the range of values of $(\sigma_1 - \sigma_3)/\sigma_n$ will be 1.30–2.06. Analysis of the

experimental data for the ‘last’ brittle point and the ‘first’ ductile point shows that the range of values actually lies between 1.37 and 2.01. In the case of the 2 limestones which are known to have high ϕ_b values (see Table 1), the values of $(\sigma_1 - \sigma_3)/\sigma_n$ across the transition range from 1.82 to 2.01, suggesting ϕ_b values in the range 34° – 36° . This is very realistic.

The brittle–ductile transition is such a significant state for rocks that it is of value to develop relationships from which further information can be obtained. For example, it would be very useful for the field interpretation of joint and fault orientations if the *conjugate shear angle* (2β) between conjugate failure planes could be determined. Likewise, an expression for the stress level required to reach the *transition pressure* for a given rock would be of considerable value since this pressure when corrected for temperature and time (see Price, [41]) may well represent the conditions in the crust when the particular rock last became a brittle solid, or, in the case of sedimentary rocks, when the particular rock was under the maximum load of sediments.

It can be shown from equations (18) and (32) that the total friction angle θ_t exhibited at the brittle–ductile transition is a function only of the basic friction angle ϕ_b , assuming that the critical state line represented by $\phi_c = 26.6^\circ$ has the same gradient for all rocks. Thus:

$$\theta_t = 1/3(5\phi_b - 2\phi_c). \quad (33)$$

A quick experimental check of this equation indicates that for the majority of rocks—particularly silicate rocks—the value of θ_t should be 32.3° , since ϕ_b is most commonly 30° . This almost exactly coincides with the value frequently quoted in the literature (i.e. $\mu = 0.65$, Mogi [4] p. 225). It also explains how a carbonate rock such as limestone with ϕ_b between 35° and 40° may have θ_t as high as 41° – 49° (i.e. $\mu \approx 1.0$, Mogi [4] p. 225). Apparently shale might have a value of θ_t as low as 19° , assuming that $\phi_b = 22^\circ$ is correct for this rock.

It can be shown from equations (9) and (27) that the angle (2β)* between the conjugate failure surfaces is given by the following expression:

$$\sin 2\beta = 2(\tau/\sigma_n) \exp \left[-\frac{1}{50n} (\tan^{-1} (\tau/\sigma_n) - \phi_c) \right] \quad (34)$$

where $n = 0.43$ is the ratio between \log_e and \log_{10} . The gradient of the Mohr envelope (ϕ) is also found from the above expression by equating $\cos \phi = \sin 2\beta^*$. This is apparent from equation (11). The above expression can be simplified for the case of the brittle–ductile transition by substituting equation (33). Thus:

$$\sin 2\beta = 2 \tan \theta_t \cdot \exp \left[-\left(\frac{\phi_b - \phi_c}{13.03} \right) \right]. \quad (35)$$

The common value $\phi_b = 30^\circ$ suggests a value of $2\beta = 76^\circ$; but it is clear that the angle between the failure planes is very sensitive to the value of ϕ_b , particularly when this approaches 26.6° , in which case $2\beta = 90^\circ$.

*It should be emphasised that the value of β is strictly relevant to the two-dimensional case as represented by the Mohr construction, namely when $\sigma_2 = \sigma_3$. The conjugate surfaces developed under these so-called ‘triaxial’ conditions are actually slightly curved, while the conjugate failure surfaces developed under three-dimensional stress states with $\sigma_1 > \sigma_2 > \sigma_3$ are *planar* and intersect along lines parallel to σ_2 .

In order to find an expression for the ratio σ_1/σ_3 at the brittle-ductile transition, it is necessary to obtain a relationship between the angle θ_t subtended by the point of tangency, and the angle α_t subtended by the top point E of the transition circle (angle EOF, Fig. 13). It can be shown from the geometry of the transition stress circle that:

$$\tan \theta_t = \frac{\tan \alpha_t \cdot \sin 2\beta}{1 - \tan \alpha_t \cdot \cos 2\beta}$$

whence

$$\tan \alpha_t = \frac{\tan \theta_t}{\sin 2\beta + \cos 2\beta \cdot \tan \theta_t} \quad (36)$$

If 2β is evaluated from equations (35) and (33), and the value obtained substituted in equation (36) then it is possible to estimate the value of σ_1/σ_3 at the transition from the following simple relationship:

$$\sigma_1/\sigma_3 \text{ (transition)} = \frac{1 + \tan \alpha_t}{1 - \tan \alpha_t} \quad (37)$$

We are now close to obtaining the desired expression for the mobilized transition pressure (σ_n transition) represented by point P in Fig. 13. Since this pressure is clearly dependent on the strength of the rock concerned, and not just on the appropriate value of ϕ_b , it is necessary once again to make use of equation (24). This can be rearranged to give:

$$\frac{\sigma_1 - \sigma_3}{\sigma_n} = \frac{\sigma_c}{\sigma_n} (M \sigma_3/\sigma_1 + 1.0).$$

Hence, at the transition, with equation (31) we have:

$$\sigma_n \text{ (transition)} = \sigma_c (M \sigma_3/\sigma_1 + 1.0) \times \exp \left[- \left(\frac{\phi_b - \phi_c}{13.03} \right) \right] \quad (38)$$

The above equations will now be evaluated so that the predicted transition pressures can be compared with the experimentally measured values. It is necessary to know 3 things about a rock before the transition pressure can be estimated. A value of ϕ_b is required to estimate the total friction angle θ_t at the transition. Values for the unconfined compression strength σ_c and the gradient M , Fig. 14, equation (24), are also required.

Example

- (1) Solenhofen limestone $\phi_b = 35^\circ$ $M = 3$ $\sigma_c = 250 \text{ MN/m}^2$ (2.5 kbar),
- (2) Oak Hall limestone $\phi_b = 35^\circ$ $M = 7$ $\sigma_c = 260 \text{ MN/m}^2$ (2.6 kbar),
- (3) Westerly granite $\phi_b = 30^\circ$ $M = 30$ $\sigma_c = 240 \text{ MN/m}^2$ (2.4 kbar).

Evaluating equations (33), (35), (36), (37) and (38), the following values are obtained:

	θ_t	2β	$\tan \alpha_t$	σ_1/σ_3	σ_n (transition)
(1)	40.6°	64°	0.67	5.1	210 MN/m ² (2.1 kbar),
(2)	40.6°	64°	0.67	5.1	320 MN/m ² (3.2 kbar),
(3)	32.3°	76°	0.56	3.6	1730 MN/m ² (17.3 kbar).

The values of σ_n (transition) obtained above are very close to the values reported in the literature. For example, Byerlee ([5] p. 3636) reports that the fracture and friction envelopes for Westerly granite intersect (at the transition) when the normal stress is about 1750 MN/m² (17.5 kbar).

Before leaving the brittle-ductile transition, it is of interest to return to Fig. 17, showing the Mohr envelope for Solenhofen limestone. The curved envelope which passes close to the 4 experimental points, is the predicted frictional strength obtained from equation (30) with an assumed ϕ_b value of 35°. The theoretical transition where the 2 curves intersect occurs between the sixth and the tenth stress circles.

The 'last' brittle failure and the 'first' ductile failure were actually recorded by Byerlee between the seventh and eighth stress circles, almost as predicted.

It should be noted that the predicted envelope for the faults has been extended as a dotted line beyond the transition. Whether the intact rock and faults are governed by equation (27) (fracture strength) at stresses higher than the transition, or by equation (30) (frictional strength), is a matter for conjecture. Mogi [42] has suggested that there may indeed be two distinct types of behaviour for rocks which he termed A-type and B-type according to whether they followed the fracture envelope or the frictional envelope above the transition. In many ways it is easier to imagine that the individuality of a rock as expressed by ϕ_b is lost 'in the melting pot' when it becomes ductile, so that all follow the same law, equation (27). This will be an interesting topic for further investigation.

Analogy to the behaviour of clay

The fracture envelopes and the friction envelopes of rock are in some ways analogous to the peak strength envelopes of over-consolidated (O.C.) and normally-consolidated (N.C.) clays. Clay that has been historically consolidated under a greater effective pressure than existing at present is over-consolidated, just as all rocks are over-consolidated, most of them enormously so. However, as O.C. clays and rocks are re-stressed, they reach a point when they are again in a normally consolidated state relative to the historic maximum effective pressure. The existing mineral structure and

cement bonding are in effect the rock's memory of past conditions.

In the case of clay this normally consolidated condition is reached when the O.C. and N.C. envelopes merge, both to follow (in the case of drained tests) the N.C. envelope up the appropriate critical state line. For rocks this stage is represented by the brittle-ductile transition when both the fracture and friction envelopes are coincident. The friction envelope represents a material whose cohesive bonds have been broken (locally) by fracture. It seems possible, and it is certainly an attractive hypothesis, that at high temperatures the fracture and friction envelopes merge on the critical state line. If all rocks lost their individual values of ϕ_b at high temperature such that $\phi_b = \phi_c$, then this point of merger would also represent the brittle-ductile transition. This point needs further investigation.

In the case of igneous and metamorphic rocks, the brittle-ductile transition may possibly give a measure of the effective stress operating when the rock crystallized into a solid brittle material *on the last occasion*. The mobilized normal pressure (σ_n transit. pressure P , Fig. 13) will not of course be the exact pre-consolidation pressure, because it has to be corrected for time and temperature effects. Rock is brittle over a smaller range of stress when the rate of strain is very slow and when at elevated temperatures, as shown by Price [41]. The value of σ_n (transition) therefore represents an equivalent pre-consolidation pressure, relevant to relatively high rates of strain and to room temperature, and is therefore an overestimate of the historic pressure. In the case of sedimentary rocks this pressure may also represent an equivalent pre-consolidation pressure, relevant to the maximum superincumbent load to which the rocks have been subjected. A smaller temperature correction might perhaps be in order in this case.

PART II

FULL SCALE BEHAVIOUR IN THE EARTH'S CRUST

The enormous step involved when extrapolating laboratory scale tests on faults of a few cm² in area to crustal faults perhaps 10 orders of magnitude larger, implies that there may be some justification for using empirical laws such as those developed in Part I. However, it is obviously important that these empirical laws are sensitive to those factors known to influence laboratory results. For example, in the case of joints or faults; the rock strength, joint weathering, surface roughness, presence of water (and water pressure), and the effects of time are all known to influence the shear strength. It is of extreme importance to investigate their effects on a larger scale.

Numerous compression tests have indicated that the laboratory size sample of a few centimetres size may give an overestimate of strength by a factor of up to 5 or 10, when compared to the results of *in-situ* tests on rock blocks of a metre or more in size. As noted by Brace [43], this scale effect appears to die out for large sample sizes. However, these recent investigations of scale effects in the field of rock mechanics [44-46] are inevitably limited to moderate stress levels because of the extreme size of the *in-situ* specimens. It is perhaps possible that at several kilometers depth there is less scale effect than indicated by these tests, due to reduced *pore* and *flaw* volumes.

Inevitably, a discussion of full scale behaviour in the Earth's crust must be on a hypothetical plane since few hypotheses can be checked with certainty. However, since an understanding of full scale behaviour is (or should be) the object of laboratory scale tests and theories, it is obligatory to attempt to extrapolate the preceding theoretical models at least to some depth into the crust.

The conjugate shear angle

It is convenient to start looking at those full-scale features that are presently exposed at the surface, namely joints and faults. These features provide us with a record of *previous* conditions at depth. Hopefully, they also provide a picture of *present* conditions at depth in some parts of the Earth's crust.

Conjugate sets of faults and shear joints intersect along lines parallel to the former intermediate effective principal stress (σ_2), and their acute angle of intersection represented by $(2\beta)^*$ is bisected by the former major effective principal stress (σ_1). The angle (2β) reflects the strength of the rock when these failure surfaces developed since it is related to the inclination ϕ of the envelope of fracture strength by the simple expression: $2\beta = 90 - \phi$.

Experimental observations by Brace [47] suggest that the conjugate shear angle (2β) varies gradually from about 0° to 60° as the applied stress changes from tensile to compressive. These observations are indirectly confirmed by field studies of joint patterns, in which quite small conjugate shear angles have been observed, for example 10-30° (see Secor [48, p. 635]; Badgley [49, p. 19]). In the case of *normal* and *thrust* faults Price [50, p. 59] gives values of 2β in the range 50-60°, and 40-50°, respectively, while Anderson [51] recorded values of about 36-50° for normal faults and 50° for *wrench* faults.

The range of values for 2β suggested by the theoretical linear envelope, equation (29), between the uniaxial tension and compression circles depends on the ratio σ_c/σ_t . If for convenience, values of σ_c/σ_t equal to 9 and 16 are assumed, then the hypothetical range of ϕ will be from 53° to 62° respectively. Since $2\beta = 90 - \phi$, these values suggest a range of 37-28° for the conjugate shear angles. The range of 36-60° for normal faults suggest that either the ratio σ_c/σ_t for rocks can sometimes be less than 9, or that the real curvature of the

*See footnote on p. 269.

envelope in this region should not be ignored. A curved envelope between the same two stress circles ($\sigma_2/\sigma_1 = 9$) would result in values of 2β somewhat greater than 37° with small negative values of σ_3 .

The reducing gradient of the strength envelope as σ_3 becomes positive and increases, leads to steadily increasing values of 2β as shown in Fig. 17. A condition of extreme importance to the development of joints in rock is the brittle-ductile transition. It is likely that many joint patterns, particularly those in igneous and metamorphic rocks, will reflect the stress-strength condition when the rock last became brittle (i.e. just on the brittle side of the transition). In the case of metamorphic rocks the interpretation may of course be complicated by anisotropic strength properties which will clearly affect the value of 2β under given stress conditions.

In the case of isotropic rocks, equations (35) and (33) can be used for estimating the conjugate shear angles at the transition. When $\phi_b = 30^\circ$ as commonly found, 2β should be 76° . However, if ϕ_b is as high as 40° or lower than ϕ_c (26.6°), the conjugate shear angles may range all the way from 55° to more than 90° .

Markedly planar, *orthogonal joint sets* are frequently to be found in rocks which have been subjected to tectonic loading. If the empirical model for the brittle-ductile transition can be extended to full scale processes, to extremely slow rates of strain, and to high temperatures (by changing the stress scale), then it is possible to draw some interesting conclusions concerning the physical state of the rocks during the formation of those orthogonal joints that result from shear failure.

If such joints formed at stress levels just on the brittle side of the brittle-ductile transition of the respective rocks, then values of ϕ_b would apparently need to be about equal to ϕ_c , i.e. 26.6° . Since only a relatively small number of rocks have values of ϕ_b of approximately this magnitude, it suggests that many conjugate shear joints might be formed, or at least *their planar traces predetermined*, at stress levels higher than the brittle-ductile transition. Possibly their position is predetermined by slip planes developed when the rock was in a completely ductile state as represented by the *critical state*. (All rocks should theoretically develop orthogonal conjugate shears at their critical state, whatever values of ϕ_b are involved).

Field evidence for such a theory is strong in view of the widespread occurrence of approximately orthogonal tectonic joints. In addition, their extreme planarity, often over many tens of metres, is very dissimilar to the surface appearance of, for example sheeting joints, which presumably formed in tension when the rock was in a completely brittle condition. In fact, it seems possible that some of these planar orthogonal conjugate shears also developed when the rock was in a brittle state, since on a small scale they may exhibit a rough surface texture, as if brittle failure was involved but in this case strictly controlled by the predetermined planar traces developed at an earlier point in their history.

Seismic instability and stress drop magnitudes

The joint and fault development just discussed may result in measureable seismic events, if the stress drops accompanying fracture are large enough and occur rapidly enough. A sudden major instability may cause elastic energy to be radiated such great distances that an earthquake is registered.

It appears that most earthquakes occur in the upper crust. Furthermore, over 75% of the average annual seismic energy is released by earthquakes with focal depths less than about 60 kilometers [52]. In some regions, such as California, no earthquakes with foci below the Earth's shallow crust (20-40 km under continents) have been recorded. Deep earthquakes are believed to occur in material that is not typical of their depth, for example slabs of crustal materials sinking under deep trenches.

If these deep earthquakes are removed from the data, it is found that seismic activity in general is confined to the uppermost 50 km of the earth. This implies lithostatic stress levels of up to 1000-1500 MN/m² (10-15 kbar). Significantly, the depth of a fault zone does not as a rule increase with increasing magnitude of earthquake. Rather it reaches a maximum value the thickness of the seismic crust. In California this is usually no more than 20 km, which implies a lithostatic stress level of only about 500 MN/m² (5 kbar).

Two sources of instability are usually referred to (Nur [52]; Brace [43]). Firstly there is the *brittle failure* of intact rock in compression, and secondly *stick-slip* along the pre-existing faults. Stick-slip is an oscillating mechanism in which stress rises during the period of fault stick, to be followed by slip, a new build up of stress, the process repeating itself many times. In laboratory tests on many different rock types, stress drops of several hundred MN/m² (several kbars) can occur at each slip event if the confining pressure is quite high—i.e. several hundred MN/m². This magnitude of

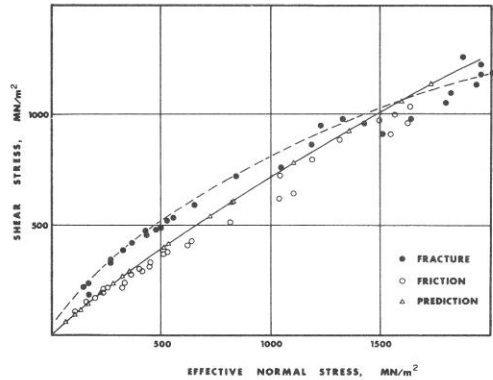


Fig. 18. Fracture strength, frictional strength and predicted frictional strength for Westerly granite based on experimental data reported by Byerlee ([5], Figs. 7 and 8). The predicted strength is based on equation (30), with an assumed value of $\phi_b = 30^\circ$.

stress drop appears to be far greater than that estimated during major earthquakes, typically about 3–6 MN/m² (30–60 kg/cm²) for magnitude 6.8–8.3 events [52]. The influences of the stiffness, damping and inertia of the moving fault blocks have been suggested as possible limiting factors *in-situ* [5]. In addition, it should not be forgotten that the fault intersects the boundary of a laboratory specimen, whereas in the Earth only a finite—though probably very large—part of the fault moves during an earthquake.

Figure 18 illustrates the difference between fracture strength and frictional strength and the associated stress drop suggested by laboratory tests on Westerly granite [5]. In the same figure the frictional strength predicted using equation (30) is shown. This is based, as before, on the measured values of $(\sigma_1 - \sigma_3)$ and (σ_3) at fracture (Byerlee [5], Fig. 8), and an assumed fault angle of 30°.*

It can be seen from Fig. 18 that the *apparent* stress drop available due to brittle fracture of the intact rock is actually maximum at an effective normal stress of about one third that needed to reach the brittle–ductile transition. The maximum value indicated by these small scale laboratory tests is of the order of 150 MN/m² (1.5 kbar).

In fact, the ‘instantaneous’ stress drop may be even larger since the *peak strength of the fault* is not mobilized at fracture, but after a finite displacement. The trough in the shear stress–displacement curve represents a *larger stress drop* than the net loss of strength between *fracture peak* and the *friction peak*. As far as earthquake sources are concerned, the maximum stress drop will be the critical one as this stress is released very rapidly. The stress drop due to fracture of intact rock is in fact larger than the value suggested by subtracting the expression for (τ) in equation (30) from that of equation (27).

At both lower and higher stress levels, the apparent stress drop reduces, becoming zero at the transition pressure and equal to the cohesion of the intact rock at zero confining pressure. As pointed out by Byerlee [5], if the Coulomb theory of fracture were valid for rock at high stress, the stress drop between the fracture envelope and the friction envelope should be a constant representing the cohesive strength of the rock. Clearly, this theory is not valid here.

The above sources of instability produce on a laboratory scale single stress drops one to two orders of magnitude larger than those apparently occurring in the largest earthquakes. The excessively large stress-drops encountered in laboratory scale *stick-slip* events can

*The frictional data points obtained by Byerlee were actually for artificial tension fractures generated in blocks of Westerly granite, obtained by coring triaxial cylinders with the fracture at about 30° to the axis. It has been assumed that $(JRC) = 20$ is also valid for these surfaces. According to Byerlee [5], the very high stresses applied in these tests reduce the experimental accuracy of the normal and shear stresses to $\pm 3.5\%$ at confining pressures up to 500 MN/m² (5 kbar), and $\pm 9.5\%$ at confining pressures up to 1000 MN/m² (10 kbar). This might explain the considerable scatter of experimental results at high stress.

perhaps be explained by invoking arguments concerning *in situ* damping and inertial effects. However, the stress drop resulting from *brittle fracture* is apparently too large as an earthquake source mechanism, unless:

- (i) it occurs at very high stresses approaching the transition pressure;
- (ii) it is smaller than indicated by laboratory tests, due to a scale effect;
- (iii) it is smaller than indicated by laboratory tests, due to the finite area of fault involved in any seismic event.

The first argument appears feasible in one respect in that the volumetric dilation would probably be less marked at these high stresses, thereby resulting in less ‘dilation hardening’. This is a phenomenon caused by rapid pore pressure decreases accompanying the volumetric dilation of saturated rock [43]. However, if crustal rocks are in any way typified by Westerly granite, the effective normal stress might need to be as high as 1500 MN/m² (15 kbar) to limit the stress-drop sufficiently. This would imply an effective confining pressure of the order of 900 MN/m² (9 kbar); just below that required to reach the brittle–ductile transition in the laboratory samples of Westerly granite (Fig. 18). When interpreted as a lithostatic load, this implies a depth in the crust of the order of 40 km.

A table listing the depths of earthquakes known to have occurred on active (therefore pre-existing) faults given by Nur [52], shows 12 earthquakes having focal depths of between 1.4 and 10 km, and 21 earthquakes having focal depths of from 10 to 20 km. If it is possible that earthquakes caused by brittle fracture can also occur at these shallow depths, then the brittle–ductile transition pressure of rocks *in situ* must apparently be markedly less than that demonstrated by, for example, Westerly granite. This would be the case if a scale effect existed, sufficient to reduce the shear strength of rock even at high stress levels.

Experimental and theoretical scale effect

As discussed earlier, the scale effect that has been demonstrated in rock mechanics is limited to moderate stress levels, due to the large size of the *in situ* specimens. However, accepting this experimental limitation it is of interest to see how equation (7) and the families of shear strength envelopes presented in Fig. 5 fit into the experimental findings.

Figure 5 demonstrates that a scale effect on compressive strength—which would also affect the joint wall compressive strength (*JCS*)—would have a marked effect on the shear strength predicted for rough-undulating joints ($JRC = 20$), but a minimal effect on smooth, nearly planar joints ($JRC = 5$). There should thus be minimal or zero scale effect on residual strength, and maximum scale effect on the peak strength of the roughest fracture surfaces which are probably analogous to faults in their immediate post-fracture state.

A comprehensive series of scale effect tests in quartz diorite have recently been reported in the rock

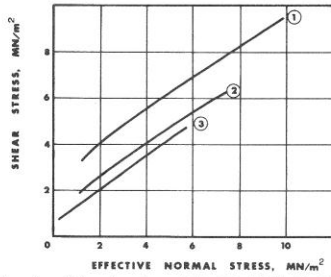


Fig. 19. Results of *in situ* shear tests on joints in quartz diorite, after Pratt *et al.* [44]. Envelope (1) represents specimens with an average area of approx 200 cm², (2) an average area of 1500 cm², and (3) an average of 5000 cm².

mechanics literature. Unconfined compression strength tests reported by Pratt *et al.* [53] included sample lengths from about 5 cm to 275 m. Direct shear tests performed on natural joints in the same rock type described by Pratt *et al.* [44] included joint areas ranging from 60 cm² up to 5000 cm².

The first study showed that the *unconfined compression strength* dropped from about 60 or 70 MN/m² (600 or 700 kg/cm²) for 5 cm long specimens down to about 7 MN/m² (70 kg/cm²) for 90 cm long specimens. Further increases in specimen length to 275 cm did not appear to indicate any scale effect beyond a length of about 100 cm.

The second study concerning *shear strength of joints* in the same rock, showed roughly 40% drop in peak shear strength over the range of surfaces tested. If these surface areas are converted to representative lengths by taking the square root of the areas, the size range is seen to be approx 8 cm to 70 cm. The shear strength in fact showed a less marked scale effect than unconfined compression strength, but significantly the shear strength scale effect did not apparently die out within the size range of specimens tested.

Figures 19 and 20 show a comparison of experimental shear strength envelopes (curves 1, 2 and 3) reported in the above study [44], and their theoretical counterparts based on equation (7). Values of (*JRC*) equal to 20 were assumed in each case. This might well be an over-estimate of roughness. (It was not described by the authors). The values of (*JCS*) of 54, 23 and 13

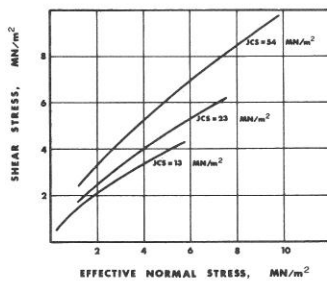


Fig. 20. Theoretical peak shear strength envelopes obtained from equation (7) (Fig. 5) with values of (*JCS*) as shown, and assumed values of $\phi_b = 30^\circ$, and (*JRC*) = 20.

MN/m² (540, 230 and 130 kg/cm²) were obtained by back-calculating using equation (7), with an assumed value of $\phi_b = 30^\circ$, and a single value of τ/σ_n taken from the middle of each of the 3 experimental curves. The theoretical envelopes extrapolated from these single experimental results show fairly similar trends to those measured. The upper envelope is a little too steep, the middle envelope almost identical, and the lower envelope a little too flat and curved.

The representative lengths (square root of area) for the shear tests recorded in Fig. 19 were approx 14, 39 and 71 cm, respectively. The unconfined compression strength measured on 5 cm long specimens corresponds approximately to the *JCS* value back calculated for the 14 cm shear tests. The unconfined compression strength measured on 30–45 cm long specimens corresponds approximately to the *JCS* value back calculated for the 71 cm shear tests. If this approximate 1:2 or 1:3 length ratio holds for larger specimens, it suggests that the shear strength scale effect might in theory die out when the representative lengths are 2 to 3 times that of the largest compression specimens just sensitive to the scale effect—which was apparently about 100 cm according to Pratt *et al.* [53]. This would imply that the shear strength scale effect might die out for joint lengths in excess of 2 to 3 m.

One significant piece of data can be used to support this tentative hypothesis. The direct shear tests performed on rough-undulating tension fractures generated in various weak, brittle model materials reported by Barton [17, 54] represented full scale test lengths ranging from about 2–30 m when a full scale unconfined compression strength of 50 MN/m² (500 kg/cm²) was assumed for *each* scale of test. No shear strength scale effect was evident over this range of simulated specimen sizes with the assumed constant σ_c value [17, Fig. 4]. Perhaps all the shear strength scale effect is concentrated within the first 2 m of joint lengths. In the case of smoother and more planar joints, the scale effect might possibly die out within smaller dimensions than this.

The unconfined compression strength scale effect that apparently dies out for sample lengths in excess of 1 m was also observed by Bieniawski and Van Heerden [46] for coal. However, the maximum 10-fold reduction in strength has not been approached by the stronger rock types. As noted earlier, it is a matter for speculation whether these scale effects apply to extremely high stress environments, in which porosities and microscopic and macroscopic flaws will possibly be much reduced in magnitude.

Possible significance of scale effect to earthquakes

The discussion presented earlier indicated an apparent lack of fit between stress drop magnitudes observed in the laboratory and those back-calculated from major earthquakes. Those observed in laboratory size samples were apparently much larger than those back-calculated from major seismic events. According to the review article by Nur [52], stress drops of from 1 to

The Shear Strength of Rock and Rock Joints

10 MN/m² (10–100 bars) may be realistic for major earthquakes. The upper limit corresponds to the 100 year periodicity theory for the San Andreas fault, in which shear stress is assumed to build up at a rate of about 0.1 MN/m² (1 bar) per year, releasing a very large earthquake approximately once in every 100 years.

If we tentatively apply the above findings on scale effect to seismic events, some interesting results are obtained. Hypothetical τ , σ_n envelopes can be generated using equation (14) for fracture strength, and using equation (8) for frictional strength. For convenience, the earlier assumptions of a 30° fault angle, $\phi_b = 30^\circ$, and $JRC = 20$ were used. Firstly, a 'laboratory' test was simulated with a rock having an assumed unconfined compression strength (σ_c) of 250 MN/m² (2.5 kbar), and a (k) value, equation (14), of 5.0. The corresponding fracture and friction envelopes intersect at an effective normal stress of 2100 MN/m² (21 kbar). This hypothetical brittle-ductile transition occurs at a confining pressure (σ_3) of about 1250 MN/m² (12.5 kbar), equivalent to a lithostatic overburden of about 50 km. As seen from Fig. 21, the apparent maximum stress drop available is about 120 MN/m² (1.2 kbar). It is only when the stress level is extremely high that the stress drop becomes less than 10 MN/m² (100 bars). The depth would need to be of the order of 45–50 km.

If, due to a minor scale effect, the *in situ* unconfined compression strength is only half of the laboratory value (i.e. 125 MN/m² or 1.25 kbar), and assuming the same coefficient (k) is applicable, it is found that the hypothetical brittle-ductile transition occurs at an effective normal stress level of half the previous value. The shear stress required is also half, and the maximum available stress drop is only 60 MN/m² (0.6 kbar). A stress drop of less than 10 MN/m² (100 bars) would occur at a hypothetical depth of only 22–25 km.

If this example is extended and we now assume a 10-fold drop in compressive strength due to a scale

effect, then the above estimates of the brittle-ductile transition pressure are reduced to about 125 MN/m² (1.25 kbar), equivalent to a lithostatic overburden of about 5 km. The apparent *maximum* stress drop available is in this case only about 12 MN/m² (120 bars), similar to that occurring during a very large earthquake.

It may therefore be reasonable to tentatively conclude that *if no scale effect exists at depth*, earthquakes of the brittle-failure-of-intact-rock variety will be limited to depths close to those required for the onset of ductility. On the other hand, if a significant scale effect does exist—even at depth—then earthquakes caused by brittle failure may well occur at quite shallow depths, even in the stronger rocks.

It is interesting to note that with the hypothetical models used above, the three brittle-ductile transitions have a constant value of $\arctan(\tau/\sigma_n)$ of 33.7° ($=\theta$). This is 1.4° higher than predicted by equation (33). The reason for the small discrepancy is due to the assumption of a constant 30° fault angle for this hypothetical example, when in reality the angle changes with the inclination of the shear strength envelope.

Strength corrosion due to water

This discussion on the effects of scale on shear strength would be incomplete without consideration of the dual role of water, namely the possible *strength corrosion*, and the more obvious effective stress effects caused by dilation.

A review of the effect of water on the shear strength of rock joints and its related effect on the tensile and compressive strength of rocks [18, pp. 322–326] indicated that at low-to-medium stress levels the shear strength of most smooth polished rock surfaces is unaffected or increases in strength slightly when wet. Conversely, natural or rough joint surfaces appear to reduce in strength when wet. Reductions can amount to 5–30% according to the limited data available.

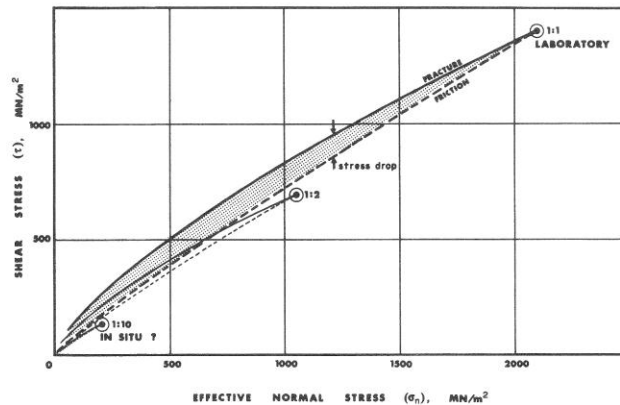


Fig. 21. Results of a hypothetical investigation of the possible effect of scale on the apparent stress drop and brittle-ductile transition pressure.

Exceptions can generally be explained by the mineralogy. For example, a smooth polished minor fault in a quartz-rich rock (massive crystal structure), would normally be unaffected or would increase slightly in shear strength when wet. However, the presence of a polished chlorite coating on such a surface would dominate the behaviour since layer-lattice crystal structures suffer a big reduction in shear strength when wet [55].

Detailed observations of sheared fractures in granitic gneiss reported by Jaeger [13] suggest that slickensides develop across powdered shear debris most readily when the surfaces are saturated, with consequent reduction in shear strength and a greater curvature of the strength envelope. Such changes of behaviour are not available to joints that are already slickensided.

Even when surfaces are subjected to shear stress, it is likely that on the asperity scale, local tensile failures occur. Significantly, this will be more marked for natural rough surfaces than for artificial, polished surfaces. Similarly, any crushing of shear debris (which may involve tensile failure) will occur to a much greater extent between the walls of rough joints or faults than in smooth planar joints.

Equation (7) can in fact be expressed directly in terms of the tensile strength of the rock (σ_t). If we assume, as commonly found, that $\sigma_c = 10 \sigma_t$ (approx), then equation (7) can be rewritten:

$$\tau = \sigma_n \tan \left[JRC \log_{10} \left(\frac{\sigma_t}{\sigma_n} \right) + \phi_b + JRC \right]. \quad (39)$$

For the case of a rough, undulating joint, with $JRC = 20$ and $\phi_b = 30^\circ$, this becomes

$$\tau = \sigma_n \tan \left[20 \log_{10} \left(\frac{\sigma_t}{\sigma_n} \right) + 50^\circ \right]. \quad (40)$$

If we accept that the weakening effect of water is indeed due to its adverse affect on the tensile strength of brittle materials [5], then from purely theoretical reasoning it can be seen that the peak shear strength of rough joints (high JRC) will be more affected by water saturation than smooth joints (low JRC). *If the adverse effect of moisture on tensile strength still operates under high confining pressures*, the presence or absence of water can be expected to have a marked effect on the initial post-fracture behaviour of a fault. Even when (JRC) is reduced by subsequent shearing, the presence or absence of moisture is likely to continue to affect the shear strength, due to the easier formation of slickensides in the powdered shear debris, as noted above. At a much later stage in the life of the fault when fine gouge has developed, the presence of water will have the more obvious softening effects.

According to the test results reported in the literature [18, Table VI]; [56, Figs. 3 and 4] the tensile, unconfined compression, and confined compression strength of rocks are each strongly affected by the moisture content. For unconfined tests the reduction in strength from 'completely dry' to 100% saturation may be as

much as 50%. However, between the engineering limits 'air dry' to 'saturated *in situ*', reductions of about 20–30% seem more common.

If these effects are also present at high confining pressures, then the combined effect of moisture on fracture strength and frictional strength might be expected to *reduce the effective confining pressure required to reach the brittle-ductile transition*. The end result might be analogous to, though less severe than, the scale effect discussed earlier.

If water is present in any quantity at great depth, the resultant reduction in the effective confining pressure will tend to increase the depth required to reach the brittle-ductile transition, thus acting in the opposite direction to the above *strength corrosion effect*. The real depth of the transition to ductile behaviour will presumably depend on the balance between the inter-related effects of scale, strength corrosion, effective stress, and of course temperature. The influence of the time scale must also be considered, as emphasised by Price [41].

Fault dilation and water pressure effects

Recent interest in the variations of the ratio of travel times for shear waves and compressional waves prior to seismic events [52], has again focussed attention on the *volumetric dilation* and water content changes believed to occur in the focal zone prior to fault development. This fluid migration hypothesis was suggested by Mead [57].

Brace and Martin [58] have shown how the pore pressure within a saturated rock sample will fall if the loading rate exceeds the rate at which fluid can flow into the stressed region. The resulting *dilatancy hardening* has a temporary stabilizing effect on potential failure.

The increase in specimen volume that takes place relative to simple elastic changes, is due to microcracking. The resulting volumetric dilation rate accelerates when the stress level reaches 90–95% of the fracture stress and reaches a maximum at fracture [1]. This observation is analogous to the *one-dimensional dilation* observed during shear of rough joints, fractures or faults as discussed earlier.

Nur [52] poses the question of earthquakes: "Why do they disappear at shallow depths such as along the San Andreas fault?". Possibly the answer lies in the dilation and resulting increase in effective normal stress that may occur as a result of shear along *pre-existing faults*. Under low confining pressure, the initial volume increase caused by fault dilation might well exceed that caused by the earlier microcracking that preceded the formation of the fault. The effect of one-dimensional fault dilation is illustrated in Fig. 22.

The effective normal stress might increase from two causes. Firstly, due to the stiffness of the surrounding rock mass inhibiting displacement perpendicular to the fault, and secondly, due to the rapidly reduced water pressure accompanying any potentially rapid shear displacement. These two effects might be so marked for

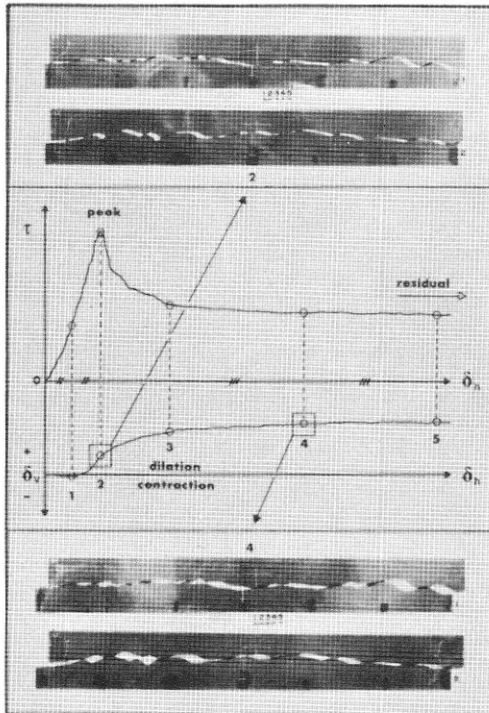


Fig. 22. Cross-sections illustrating the measured shearing paths of model tension fractures. At full-scale these models represent 30 m long fractures in a rock with $\sigma_c = 50 \text{ MN/m}^2$, sheared under a normal stress equal to 5.0 MN/m^2 in each case.

the near-surface section of a fault that a seismic event—in other words a rapid instability—is more or less inhibited. However, a slow shear displacement rate constantly controlled by the fluctuating effective normal stress can be imagined under certain circumstances. At a later period in the life of a fault the build up of fine gouge would presumably reduce the likelihood of a rapid instability even though the fault would possibly no longer be dilating.

The shear tests on model tension fractures mentioned earlier [17, 18, 54], which can be likened to tests on 30 m long sections of a rough post-fracture fault, indicated that even at the highest simulated normal stresses applied ($\sigma_n = 11 \text{ MN/m}^2$ or 110 bars, $\sigma_c/\sigma_n = 8.4$, $d_n = 7^\circ$ approx), one-dimensional dilation continued long after peak shear strength was developed, as illustrated by tests shown in Fig. 22. At the end of the shear test, after a shear displacement equal to about 8% of the length of fracture, the dilation of the surfaces had caused an increase in dimensions perpendicular to the fracture of about 0.25% of the length of fracture, in other words about 7 cm at full scale. There was no tendency for any reduction in dimensions with increasing displacement. All that happened after peak shear strength was that the *dilation rate* gradually

reduced to zero. The walls of the fracture remained propped open by the accumulated shear debris and the few remaining 'rock-to-rock' contact areas.

The increase in dimensions occurring on a full-scale fault under the same stresses as above would probably greatly exceed the 7 cm indicated for a hypothetical 30 m long fracture. Thus it can be concluded that even at the higher stresses found at a depth of 1 or 2 km, dilation along a post-fracture fault could have a significant effect in reducing the likelihood of a shallow seismic event.

CONCLUSIONS

1. The most important conclusion to be drawn from this review of frictional strength and fracture strength of rocks is that these two components of rock mass strength are related. A knowledge of fracture strength can lead directly to a surprisingly accurate estimate of frictional strength.

2. At the low levels of *effective normal stress* (σ_n) appropriate to most rock engineering problems, the frictional strength of a joint is related to the fracture strength of the intact rock by means of the *unconfined compression strength* (σ_c). The effect of confinement is presumably limited or absent due to the very small area of contact between the walls of joints in a material as rigid as rock is under these relatively low stress levels. The dimensionless ratio σ_c/σ_n controls the frictional strength at these stress levels.

3. At high levels of effective normal stress the frictional strength is related to the fracture strength by means of the *confined compression strength* which is represented by the differential stress ($\sigma_1 - \sigma_3$) at fracture. The dimensionless ratio $(\sigma_1 - \sigma_3)/\sigma_n$ (of which σ_c/σ_n is a special case, i.e. $\sigma_3 = 0$) varies relatively little over a wide range of σ_3 and results in a limited range of frictional strength at high stress levels (Fig. 1) compared to the wide range of frictional strength exhibited at low stress levels (Fig. 2).

4. At very high stress levels the shear stress required to fracture intact rock is no greater than the shear strength of the resulting fault. This important condition, known as the *brittle-ductile transition* is found to be dependent on the *basic friction angle* (ϕ_b) for the rock concerned. High values such as the $35-40^\circ$ typical of limestones cause the transition to occur at relatively low stress levels, whilst values below 25° such as for shale cause the transition to occur at relatively high stress levels. Values predicted by the empirical relationships describing frictional strength and fracture strength agree closely with experimental results reported in the literature.

5. The key to the relationship between frictional strength and fracture strength is the discovery of a *critical state* for rock. It appears from a wide survey of high pressure triaxial data that the Mohr envelopes representing the peak shear strength of intact rocks, eventually reach a point of zero gradient on crossing a certain *critical state line*. This line has a gradient of

$\frac{1}{2}$ (i.e. $\tau/\sigma_n = \frac{1}{2}$). The ultimate shear strength represented by the top point of a Mohr envelope is associated with a *critical effective confining pressure* for each rock. The major and minor principal effective stresses (σ_1) and (σ_3) associated with failure at the critical state are in the ratio of 3:1 (i.e. $\sigma_1 = 3\sigma_3$).

6. The effective normal stress (σ_n) mobilized on the orthogonal conjugate shear surfaces is found to be equal to the differential stress ($\sigma_1 - \sigma_3$) at the critical state (i.e. $\sigma_n = \sigma_1 - \sigma_3$). This happens to be the limiting value of the dimensionless ratio $(\sigma_1 - \sigma_3)/\sigma_n$ used in formulating the empirical laws of friction and fracture strength. By implication, the *one-dimensional dilation* normally associated with the shearing of joints and faults is completely suppressed if the applied stress reaches the level of the critical effective confining pressure.

7. The empirical theories of friction and fracture strength which were developed from a review of laboratory-scale tests, can also be applied to the interpretation of full-scale features. One of the most obvious areas for application is in the interpretation of joint and fault orientations in the field. An important condition for the development of such features is the *brittle-ductile transition*, below which rock will behave in a brittle manner. It can be shown that the angle (2β) between *conjugate shear planes* can in theory range from about 60° to more than 90° at the transition, depending on the *basic friction angle* (ϕ_b) of the rock. The common value of $\phi_b = 30^\circ$ suggests values of 2β of about 75° .

8. The wide-spread occurrence of approximately *orthogonal shear joints in the field* ($2\beta = 90^\circ$) and the markedly planar traces of these features may possibly be predetermined by slip planes that develop under stress levels higher than the transition. Possibly the stress levels were as high as those required to reach the critical state when the rocks were in a completely ductile state. *Orthogonal failure planes* should develop in all rocks independent of their various ϕ_b values, *if formed under critical stress conditions*.

9. Large scale rock mechanics tests designed to investigate the *effect of scale* on the compression strength and frictional strength of rocks have been analysed using the empirical theory of frictional strength. It is tentatively concluded that the scale effect on the frictional strength of joints may die out when joint lengths exceed about 2–3 m. The scale effect on compression strength appears to die out when sample sizes exceed about 1 m. However, it is possible that these scale effects may be absent or much reduced under the influence of high confining pressures in the Earth's crust, if pore and flaw volumes are significantly reduced.

10. The *stress drops* recorded in the laboratory when rock fails by brittle fracture, and the stress drops measured during stick-slip events on pre-existing 'laboratory faults' are one to two orders of magnitude larger than the stress drops of about 1–10 MN/m² (10–100 bars) back-calculated from major earthquakes. Two alternative conclusions can be drawn. If a scale

effect *does* still exist under the great pressure found in the Earth's crust, then earthquakes caused by brittle fracture may occur at quite shallow depths since the resulting stress drops would be scaled down to the level back-calculated. However, if a scale effect *does not* exist at depth, then earthquakes caused by brittle fracture will apparently be limited to depths greater than some tens of km, as only at these depths will the stress drops be as small as those back-calculated. Failure would be limited to pressures close to those required to reach the brittle-ductile transition.

11. *Strength corrosion* caused by saturation with water reduces both the compressive strength and the frictional strength of rock. Rough-surfaced joints and faults presumably reduce in strength more than smooth surface due to the adverse effect of moisture on the tensile strength of the asperities. If these strength corrosion effects also occur under high pressure and on a large scale, then the *stress drops* associated with the brittle failure of intact rock and with slip on pre-existing faults in the Earth's crust may also be reduced by the presence of moisture.

12. The *one-dimensional dilation* associated with shearing of rough pre-existing faults may explain the lack of seismicity in the upper 1 or 2 km of the crust. The dilation will tend to strengthen the fault against sudden displacement, due to the increased effective normal stress resulting from the stiffness of the surrounding rock mass. If water is present in quantity, sudden displacement of the fault may be effectively suppressed by the reduction in water pressure accompanying any dilation of the fault.

Acknowledgements—The research described in this report has been sponsored by the Royal Norwegian Council for Scientific and Industrial Research (NTNF). This support is gratefully acknowledged.

Colleagues at NGI contributed a stimulating forum for discussion of some of the more controversial topics. In particular, the author would like to acknowledge the considerable amount of helpful advice given by Jean-Hervé Prevost. Kaare Høeg kindly read the manuscript and made many valuable suggestions. Vishnu Choubey carried out a large number of direct shear tests and tilting tests on joint samples from the Oslo region, and some of the results from this parallel research project were reproduced in Fig. 6.

Received 9 February 1976.

REFERENCES

1. Brace W. F. & Byerlee J. D. Recent experimental studies of brittle fracture of rocks. *Proc. 8th Symp. on Rock Mech., Univ. of Minnesota* 1966, (Edited by Fairhurst C.), pp. 58–81 (1967).
2. Byerlee J. D. The fracture strength and frictional strength of Weber sandstone. *Int. J. Rock Mech. Min. Sci. & Geomech. Abstr.* **12**, 1–4 (1975).
3. Orowan E. Mechanism of seismic faulting. *Rock deformation Symposium*, (Edited by Griggs D. & Handin J.), Vol. 79, Chap. 12, pp. 323–345. Geological Society of America Memoire (1960).
4. Mogi K. Pressure dependence of rock strength and transition from brittle fracture to ductile flow. *Bull. Earthq. Res. Inst., Tokyo* **44**, 215–232 (1966).
5. Byerlee J. D. Frictional characteristics of granite under high confining pressure. *J. Geophys. Res.* **72**, 3639–3648 (1967).
6. Byerlee J. D. Brittle-ductile transition in rocks. *J. Geophys. Res.* **73**, 4741–4750 (1968).

The Shear Strength of Rock and Rock Joints

7. Newland P. L. & Allely B. H. Volume changes in drained triaxial tests on granular materials. *Géotechnique* 7, 17–34 (1957).
8. Rowe P. W., Barden L. & Lee I. K. Energy components during the triaxial cell and direct shear tests. *Géotechnique* 14, 247–261 (1964).
9. Patton F. D. Multiple modes of shear failure in rock and related materials. Thesis, University of Ill., (1966).
10. Patton F. D. Multiple modes of shear failure in rock. *Proc. 1st Congr. Int. Soc. Rock Mech., Lisbon, 1966*, Vol. 1, 509–513 (1966).
11. Goldstein M., Goosev B., Pyrogovsky N., Tulinov R. & Turvskaya A. Investigation of mechanical properties of cracked rock. *Proc. 1st Congr. Int. Soc. Rock Mech., Lisbon, 1966*, Vol. 1, pp. 521–524 (1966).
12. Terzaghi K. Stability of steep slopes on hard unweathered rock. *Géotechnique* 12, 251–270 (1962).
13. Jaeger J. C. The frictional properties of joints in rock. *Geofis. Pura Appl., Milano* 43, 148–158 (1959).
14. Krsmanović D. & Langof Z. Large scale laboratory tests of the shear strength of rocky material. *Rock Mech. Eng. Geol., Suppl.*, 1, 20–30 (1964).
15. Lane K. S. & Heck W. J. Triaxial testing for strength of rock joints. In *Proc. 6th Symp. Rock Mech., Rolla, MI, 1964*, (Edited by Spokes E. M. & Christiansen C. R.), pp. 98–108 (1964).
16. Patton F. D. & Deere D. U. Significant geologic factors in rock slope stability. In *Planning Open Pit Mines. Proc. Symp. Theor. Background Plann. Open Pit Mines with spec. Ref. to Slope Stab. Johannesburg, 1970*, (Edited by van Rensburg P. W. J.), pp. 143–151. Balkema, Cape Town (1970).
17. Barton N. A relationship between joint roughness and joint shear strength. *Proc. Int. Symp. Rock Mech. Rock Fracture. Nancy, Paper I-8* (1971).
18. Barton N. Review of a new shear strength criterion for rock joints. *Engng Geology* 7, 287–332 (1973).
19. Brace W. F., Paulding B. W. & Scholz C. Dilatancy in the fracture of crystalline rocks. *J. Geophys. Res.* 71, 3939–3953 (1966).
20. Wallace G. B., Slebir E. J. & Anderson F. A. Foundation testing for Auburn Dam. *Proc. 11th Symp. Rock Mech., Berkeley, CA, 1969*, (Edited by Somerton W. H.), pp. 461–498 (1970).
21. Coulson J. H. Shear strength of flat surfaces in rock. *Proc. 13th Symp. on Rock Mech., Urbana, IL, 1971*, (Edited by Cording E. J.), pp. 77–105 (1972).
22. Krsmanović D. Initial and residual shear strength of hard rocks. *Géotechnique* 17, 145–160 (1967).
23. Hutchinson J. N. Field and laboratory studies of a fall in Upper Chalk cliffs at Joss Bay, Isle of Thanet. *Stress-strain behaviour of soils. Proc. Roscoe Mem. Symp., Cambridge Univ., 1971*, (Edited by Parry R. H. G.), pp. 692–706. G. T. Foulis, Henley-on-Thames (1972).
24. Barton N. Estimation of *in situ* shear strength from back analysis of failed rock slopes. *Proc. Int. Symp. Rock Mech. Rock Fracture, Nancy, Paper II-27* (1971).
25. Ripley C. F. & Lee K. L. Sliding friction tests on sedimentary rock specimens. *Trans. 7th Int. Congr. Large Dams, Rome, 1961*, Vol. 4, pp. 657–671 (1962).
26. Hobbs D. W. The behaviour of broken rock under triaxial compression. *Int. J. Rock Mech. Min. Sci.* 7, 125–148 (1970).
27. Barton N. & Choubey V. To be published. (1976).
28. Goodman R. E. The deformability of joints. *Determination of the in situ modulus of deformation of rock. Symp. Denver, CO, 1969. ASTM. Spec. tech. publ.*, 477, 174–196 (1970).
29. Paulding B. W., Jr. Coefficient of friction of natural rock surfaces. *Proc. ASCE*, 96, No. SM2, 385–394 (1970).
30. Rengers N. Unebenheit unter Reibungswiderstand von Gesteinstrennflächen. *Diss. Tech. Hochschule Fridericiana, Karlsruhe, Ins. Bodenmech. Felsmech. Veröff.* 47, 129 (1971).
31. Jaeger J. C. Friction of rocks and stability of rock slopes. *Géotechnique* 21, 97–134 (1971).
32. Mogi K. Some precise measurements of fracture strength of rocks under uniform compressive stress. *Felsmechanik und Ingenieurgeologie* 4, 41–55 (1966).
33. Raleigh C. B. & Paterson M. S. Experimental deformation of serpentinite and its tectonic implications. *J. Geophys. Res.* 70, 3965–3985 (1965).
34. Murell S. A. F. The effect of triaxial stress systems on the strength of rocks at atmospheric temperatures. *Geophys. J. R. Astr. Soc., Lond.* 10, 231–281 (1965).
35. Hoek E. & Bieniawski Z. T. Brittle fracture propagation in rock under compression. *Int. J. Fract. Mech.* 1, 137–155 (1965).
36. Bieniawski Z. T. Estimating the strength of rock materials. *J. S. Afr. Inst. Min. Metal* 74, 312–320 (1974).
37. Cornet F. & Fairhurst C. Variation of pore volume in disintegrating rock. *Percolation through fissured rock. Proc. Symp. ISRM, Stuttgart, Paper T2-A*, (1972).
38. Vesić A. & Barksdale R. D. On shear strength of sand at very high pressures. *Symp. on Lab. Shear Testing of Soils, Ottawa, 1963. ASTM. Spec. techn. publ.* 361, 301–305 (1964).
39. Vesić A. S. & Clough G. W. Behaviour of granular materials under high stresses. *Proc. ASCE* 94, No. SM3, 661–668 (1968).
40. Maurer W. C. Shear failure of rock under axial and hydrostatic pressure. *Proc. 1st Congr. Int. Soc. Rock Mech., Lisbon, Vol. 1*, pp. 337–341 (1966).
41. Price N. J. Rheology of crustal rocks. *Geodynamics Today—A Review of the Earth's Dynamic Processes, Ottawa, 1963. Royal Society, London*, (1975).
42. Mogi K. On the pressure dependence of strength of rocks and the Coulomb fracture criterion. *Tectonophysics* 21, 273–285 (1974).
43. Brace W. F. Experimental studies of seismic behaviour of rocks under crustal conditions. *Engng Geology* 8, 109–127 (1974).
44. Pratt H. R., Black A. D. & Brace W. F. Friction and deformation of jointed quartz diorite. *Proc. 3rd Cong. of Int. Soc. Rock Mech., Denver, CO, Vol. II, A*, pp. 306–310 (1974).
45. Herget G. & Unrug K. *In situ* strength prediction of mine pillars based on laboratory tests. *Proc. 3rd Cong. of Int. Soc. Rock Mech., Denver, CO, Vol. II, A*, pp. 150–155 (1974).
46. Bieniawski Z. T. & Van Heerden W. L. The significance of *in situ* tests on large rock specimens. *Int. J. Rock Mech. Min. Sci. & Geomech. Abstr.* 12, 101–113 (1975).
47. Brace W. F. Brittle fracture of rocks. *State of Stress in the Earth's Crust* (Edited by Judd W. R.), pp. 111–178. Elsevier, NY (1964).
48. Secor D. T. Role of fluid pressure in jointing. *Am. J. Sci.* 263, 633–646 (1965).
49. Badgley P. C. *Structural and Tectonic Principles*. Harper & Row, NY, (1965).
50. Price N. J. *Fault and Joint Development in Brittle and Semi-Brittle Rock*. Pergamon, Oxford (1966).
51. Anderson E. M. *The Dynamics of Faulting and Dyke Formation with Application to Britain*, 1972 edn. Hafner, NY (1951).
52. Nur A. Tectonophysics: the study of relations between deformation and forces in the earth. *Proc. 3rd Cong. of Int. Soc. Rock Mech., Denver, CO, Theme II, General report, Vol. I, A*, pp. 243–317 (1974).
53. Pratt H. R., Black A. D., Brown W. S. & Brace W. F. The effect of specimen size on the mechanical properties of unjointed diorite. *Int. J. Rock Mech. Min. Sci.* 9, 513–529 (1972).
54. Barton N. A model study of rock-joint deformation. *Int. J. Rock Mech. Min. Sci.* 9, 579–602 (1972).
55. Horn H. M. & Deere D. U. Frictional characteristics of minerals. *Géotechnique* 12, 319–335 (1962).
56. Broch E. The influence of water on some rock properties. *Proc. 3rd Cong. of Int. Soc. Rock Mech. Denver, CO, Vol. II, A*, pp. 33–38 (1974).
57. Mead W. J. The geologic role of dilatancy. *J. Geology* 33, 685–698 (1925).
58. Brace W. F. & Martin R. J. A test of the law of effective stress for crystalline rocks of low porosity. *Int. J. Rock Mech. Min. Sci.* 5, 415–426 (1968).